



# Behaviour of Deteriorated Reinforced Concrete Columns under Elevated Temperatures

Lipi Mishra \* and Umesh Kumar Sharma, Department of Civil Engineering, Indian Institute of Technology, Roorkee 247667, India

**Received:** 18 July 2022/**Accepted:** 19 December 2023/**Published online:** 26 January 2024

**Abstract.** Corrosion of reinforcement is the primary causal factor for premature deterioration of reinforced concrete (RC) structures. Exposure to elevated temperatures such as fire events can further exacerbate the integrity of the structure. The cumulative impact of the presence of corrosion and exposure to elevated temperatures on the behaviour of short RC columns constitutes the objective of present study. An experimental investigation was conducted to evaluate the effect of the degree of corrosion on the behaviour of RC short columns exposed to elevated temperatures. Total twenty-one RC short square column specimens were cast. Twelve columns were corroded to 10% and 20% degree of corrosion in accelerated corrosion process. Subsequent to completion of the corrosion process, columns were subjected to elevated temperature exposure (500°C and 800°C) in an electric furnace. Uncorroded specimens underwent the same thermal exposure regime. Afterwards uniaxial compression test was carried out. The results indicated that corrosion had pronounced effect on the ductility and residual load-bearing capacity of the columns upon exposure to high temperatures. Significant loss of cross section in the transverse reinforcements led to compromised lateral restraint in corroded columns. Columns with 20% corrosion had brittle failure. Role of stirrup design and layout in this aspect should be further investigated. Further research is recommended for detailed studies on the heat transfer mechanism in corroded RC columns when exposed to high temperatures.

**Keywords:** Reinforced concrete, Columns, Corrosion, Fire, Elevated temperature, Thermal gradient

## Abbreviations

$P_0$	Peak load for control column (kN)
$P_{max}$	Peak load for columns other than control column (kN)
$P_{max} / P_0$	Peak load ratio of a column
$P_y$	Yield strength (kN)
$\Delta u_y$	Yield displacement (mm)
$\Delta$	Ductility factor (DF)
$\Delta u_0$	Deflection at the peak load of control column (mm)
$\Delta u_{pmax}$	Deflection corresponding to the peak load of a column other than control column (mm)

\* Correspondence should be addressed to: Lipi Mishra, E-mail: [lmishra@ce.iitr.ac.in](mailto:lmishra@ce.iitr.ac.in), [lipim4@gmail.com](mailto:lipim4@gmail.com)



$\Delta u_{0.8P0}$	Deflection at 80% of peak load of the control column (mm)
$\Delta u_{0.8P}$	Deflection at 80% of peak load of a column other than control column (mm)
$\epsilon_{P0}$	Strain at peak load for control column
$\epsilon_{Pmax}$	Strain at peak load for columns other than control column
$\epsilon_{Pmax} / \epsilon_{P0}$	Strain ratio at peak load of a column
$\epsilon_{0.8P0}$	Strain at 0.8*peak load for control column
$\epsilon_{0.8P}$	Strain at 0.8*peak load for columns other than control column
$\epsilon_{0.8P} / \epsilon_{0.8P0}$	Post peak strain ratio of a column when the load value drops to 80% of the peak load

## 1. Introduction

Reinforced concrete (RC) structures are susceptible to exposure to ever-increasing hostile environmental conditions [1–3], such as chloride attack (due to exposure to saline environment, usage of deicing salt, etc.), carbonation, sulphate attack; and hazardous events such as fire. These can lead to inferior structural performance and reduced service life of such structures. The most prevalent mechanism that deteriorates RC structures is the corrosion of the reinforcing steel. The primary sources responsible for steel reinforcement corrosion are chloride attack and carbonation. With rapid urbanization, the qualities of river and ground water are declining due to infiltration by polluting agents from untreated industrial effluents, poor wastewater discharge management, etc. [1, 2]. Use of chloride contaminated water in concrete casting results in premature corrosion of the RC structures. Furthermore, the concentration of atmospheric carbon dioxide is rising substantially with each passing year [3]. This leads to higher carbonation rates observed in existing RC structures, making the embedded steel vulnerable to premature corrosion. Exposure to fire in a RC structure with pre-existing corrosion can further degrade its structural integrity.

A highly alkaline environment (pH > 12.5) usually prevails in concrete, forming a passive layer over the embedded steel, preventing its rapid corrosion. Chloride ions remove the protective passive oxide layer and further facilitate the corrosion process. It is well-researched that corrosion products occupy a larger volume than parent steel. The accumulation of expansive rust exerts tensile stress on surrounding concrete, which leads to cracking and spalling of concrete. The consequences of reinforcement corrosion are multiple: dissolution of steel causing loss of bar cross-section [4]; decline in compressive strength of the concrete, cracking, and spalling [5]; deterioration of mechanical properties of steel bars [6]; diminished bond strength at the steel–concrete interface [7]. Thus, corrosion-induced damages at the material level adversely affect the structural performance of RC elements.

Columns are the most critical components of any RC structure, that are paramount to the overall stability of the structural system. Despite numerous studies on corroded RC beams [8, 9], there are relatively fewer experimental studies on effects of corrosion on the load bearing capacity and deformation behaviour under load of RC columns [10]. The exposure conditions for beams and columns vary due to their location in structures and accessibility to aggressive substances. While beams are subjected to flexural stresses, columns are primarily designed to carry compressive loads. The presence of tensile stresses in beams may aid in crack propagation, thus providing pathways to corrosive agents to reach the rein-

forcing steel, accelerating corrosion process. Slender columns are designed to resist bending moment and shear as well; however, the current study pertains to only axial compression in columns. The impact of corrosion on the behaviour of RC columns have been investigated by researchers. Uomoto and Misra [5] observed reduction in residual compressive strength of RC columns with increase in corrosion level. They attributed it to the combination of two effects: reduction of effective area and strength of reinforcing bars; and formation of cracks reducing the effective area of the column and the degree of restraint the covering concrete provides to the steel bars. Rodriguez et al. [11] performed experimental studies on RC columns contaminated with 3% calcium chloride by weight of cement. Current density of 100 A/cm<sup>2</sup> was supplied over 100 days to 200 days to obtain the required level of corrosion. The compressive bearing capacity of the columns reduced by around 25% for 100 days and around 40% for 200 days of exposure, respectively. The mean axial strain corresponding to the ultimate load reduced by about 33% as the exposure duration increased from 100 days to 200 days. Revathy et al. [12] studied behaviour of RC columns under accelerated corrosion. The ultimate compressive strength of columns reduced by 3% and 12%, while the ultimate axial strain declined by 2% and 5% and the reduction in ductility was found to be 1.5% and 9% for corrosion degrees of 10% and 25%, respectively. Lee et al. [13] and Bae et al. [14] studied the effects of corrosion on RC columns. Their studies showed that corrosion affected the ductility of the specimens more significantly in comparison to their residual compressive strength. Lee et al. [13] reported a reduction of 6.62% in compressive strength for 7.5% corrosion and a decline in ductility ratio from 9.9 to 2.7. Tapan et al. [15] conducted study on the effects of corrosion at different locations in RC columns. They concluded that compared to corrosion of reinforcement in compression, the corrosion of tension reinforcement results in more reduction of strength. The study agrees with the aforementioned discussion on the process of corrosion in beams and columns. The presence of tensile stresses is more conducive to corrosion initiation and propagation. Wang et al. [16] had reported similar results in his experimental study for corroded columns with higher eccentricities. Xia et al. [17] reported decrease in compressive strength and corresponding axial strain of RC columns with increase in level of corrosion. They observed that stirrup spacing, and eccentricity of load applied considerably affect the compressive strength of the corroded columns. Vu et al. [18] studied the effects of corroded transverse reinforcement on RC columns. They reported that with the increase in level of corrosion, there was pronounced reduction in the strength and ductility of the columns. They observed steeper slope in the stress–strain curve along the post-peak section, indicating brittle failure. The deleterious effect of corrosion was observed to affect axial strain at the peak load and ultimate strain more significantly compared to its effect on the compressive strength. Wu et al. [19] and Li et al. [20] studied the performance degradation of RC columns corroded under sustained loads. Both studies observed that with rise in level of corrosion, the ultimate bearing capacity, and the corresponding longitudinal displacement decreases. Wu et al. [19] reported reduction of 22% and 35.29% in ultimate bearing capacity with average corrosion degree of 9.4% and 13.7% respectively for columns with no sustained load. While

Li et al. [20] reported 30.4% and 47.8% reduction in ultimate bearing capacity for corrosion degree of 10% and 20% respectively for columns with no sustained load. The seismic performance of corroded columns leading to reduced ultimate bearing capacity, stiffness and ductility of the columns is well established [21, 22]. Thus, reinforcement corrosion has detrimental effects on the mechanical properties of RC columns.

Another severe environmental condition to compromise the safety and serviceability of RC structures is exposure to elevated temperatures such as fire events. High temperature degrades the mechanical properties of concrete, which is ascribed to the physicochemical changes, disintegration in aggregate and cement paste and thermal incompatibility between them [23]. The ingress and storage of heat above a certain level eventually leads to temperature rise in the embedded steel reinforcements, which adversely affects their mechanical properties [24]. High temperatures may also induce spalling of concrete, which leads to section size loss as well as direct exposure of the embedded steel to high temperatures, hence compromising the load-bearing capacity of the RC element [25]. The compressive strength, tensile strength, and modulus of elasticity of concrete decline with the increase in heat exposure [26].

Numerous studies have been conducted on the effects of elevated temperature exposure on the behaviour of RC columns. The effect of various parameters on the fire resistance of RC columns is well documented. The strength of concrete [25]; type of aggregate [27]; moisture content of concrete [27]; shape and size of column cross section [28, 29]; heating scenarios such as rate of heating, duration of heating, temperature of exposure [28]; load levels, length of column and concrete cover depth, diameter of reinforcement [29]; load eccentricity [30]; detailing of reinforcement, layout of ties [30, 31]; load induced thermal strain at transient high temperatures [32, 33]; type of cooling [34]; configuration of lateral reinforcement and confinement effect [35] etc. are among the major factors that affect the fire performance of RC columns significantly. Kodur and McGrath [27] had observed that the bending of ties at 135° led to higher fire resistance in RC columns compared to columns with ties of 90° bent ends. Columns with cross ties showed improved fire resistance. Chinthapalli et al. [35] studied the fire behaviour of short RC columns in axial compression. The load carrying capacity was higher in columns having lateral reinforcements that passed through the core of the cross-section, compared to columns with only rectangular ties. The confinement effect was more significant in columns with lateral reinforcement passing through the core of the concrete. It was also more marked at elevated temperatures compared to ambient temperatures.

Very few studies have been conducted on the combined effect of presence of corrosion and exposure to elevated temperature on the mechanical behaviour of RC structural elements, most of the studies focused on RC beams. Ba et al. [36] studied the fire resistance of corroded RC beams and with increase in corrosion, rapid change in midspan deflection of beams was observed. Higher levels of corrosion caused propagation of wide cracks which made the reinforced steel bars vulnerable to fire and brittle failure occurred in those sections of the RC beams. Porcari et al. [37] observed cracking and delamination of concrete at steel-con-

crete interface due to corrosion. It led to inferior mechanical behaviour of the corroded RC beams subjected to fire. Compared to non-corroded beams, higher deflection under fire was observed in corroded beams. Sobhan et al. [38] found that when exposed to fire, corroded beams had significantly lower residual moment capacity compared to non-corroded beams. Beams with high strength concrete (HSC) showed increased spalling and resulted in lower residual moment capacity compared to other beams with lower strength concrete mix. Tariq and Bhargava [39] observed that with the increase in degree of corrosion, the yield and ultimate load capacity of corroded RC beams reduced when subjected to elevated temperatures. The target temperature of exposure had a more substantial impact on the stiffness of beams as compared to the effect of level of corrosion on it. Chandra et al. [40] studied the effects of corrosion on fire performance of RC columns. HSC corroded columns had significant loss in fire resistance due to explosive spalling and had high levels of lateral deformations in the later stages of fire exposure. At lower degrees of corrosion in normal strength concrete (NSC) columns, the corrosion cracks seemed to alleviate the spalling during fire exposure. As a result, relatively reduced lateral deformations were observed in the corroded NSC columns as compared to the non-corroded specimen.

## **2. Research Significance**

RC structures are designed to be resilient during their service life period. However, due to design flaws, subpar construction practices, inadequate material choices, the presence of harsher environmental conditions than initially anticipated, or a combination of these factors [1–3], the service life of the structures lessen. Current RC structure designs address durability requirements in a prescriptive way, thus these designs do not inherently tackle the durability concerns. It is evident in widely reported cases of premature deterioration in RC structures, corrosion of reinforcement is the primary causal factor for this deterioration. The annual direct cost of corrosion worldwide is more than US\$ 2.5 trillion [41]. Experts have estimated a net of 15% to 35% of this annual cost could be saved by application of current technologies available to curb corrosion [41, 42]. The current guidelines on the fire performance of RC structural elements pertain to pristine specimens, whereas in real RC structures the presence of reinforcement corrosion with the passage of time is reported [43]. Premature corrosion will render RC structures vulnerable to events like fire accidents. Thus, it becomes imperative to study the role of existing deterioration on the behaviour of RC structural elements upon exposure to elevated temperatures. Current experimental investigation deals with RC columns. The preceding section shows that plenty of research has been carried out to evaluate the detrimental effects of steel reinforcement corrosion, as well as elevated temperature exposure on the mechanical properties of RC columns. However, the cumulative impact of pre-existing corrosion and elevated temperature exposure on the behaviour of RC columns is seldom investigated in the literature [36–40]. The present study tries to address this research gap. This research aims to evaluate the effect of the degree of corrosion on the behaviour of RC short col-

umns when they are exposed to elevated temperatures. Twenty-one short square RC column specimens were prepared, corroded, heated in electric furnace, and tested under axial compression test. Analysis of key indicators was done to determine the impact of various parameters on the mechanical properties of the columns.

### 3. Experimental Program

#### 3.1. Specimen Preparation

The usual practice of testing pristine specimens under high temperatures might not represent the real ageing corroded RC structures exposed to elevated temperatures. To investigate the effect of reinforcement corrosion in short RC columns subjected to elevated temperatures, an experimental program was designed. Within the constraints of the available resources, a test matrix was developed. Two parameters were established for the test matrix: the target temperature and degree of corrosion. Two levels of degree of corrosion and two levels of target temperature were chosen. Based on this, a total of twenty-one column specimens were fabricated under this investigation. The dimensions of the columns were designed considering the constraints of the size of the available electric furnace in the laboratory. All columns had a height of 650 mm and square cross section of 150 mm. The middle portion of the column of 450 mm height constituted the test length. The sections of 100 mm height each at the upper and lower ends of the column were designed for providing external confinement, to eliminate any end effects during mechanical testing. The reinforcing bars in these sections were epoxy coated to avoid corrosion outside the test length region. All columns had four longitudinal bars of 12 mm diameter. The cross-sectional area of the longitudinal reinforcement was 2% of the gross cross-sectional area of the column, in compliance with the limits of IS 456 [44]. Transverse reinforcement of 8 mm diameter were provided at a spacing of 50 mm c/c throughout the test length. To avoid any local failure, a closer stirrup spacing of 25 mm c/c was provided in the external confinement regions at the top and bottom ends. In columns to be tested for corrosion, the longitudinal bars were extended out from the column surface, to provide adequate space for the supply of current through connecting clips. A clear cover of 20 mm was maintained for the reinforcements. Figure 1 shows the cross-sectional and elevation details of the columns. The aspect ratio of the columns was kept at a minimum of 1:3 as per IS 456 [44] for compression members. All the longitudinal and transverse bars were weighed before the preparation of cages. This was done to enable the gravimetric evaluation of corroded bars. K-type chromel–alumel thermocouples were installed at mid-height in the columns before casting. Each column had two thermocouples fixed at two locations in the cross section, one at the centre of the column, i.e., 75 mm from the surface, and the second one at the cover-core interface.

Concrete mix of grade M30 (Table 1) and reinforcement bars of yield strength 490 MPa (Table 2) were employed for all specimens. Concrete mix proportion was designed in accordance with IS 10262:2009 [45] for moderate environmental expo-

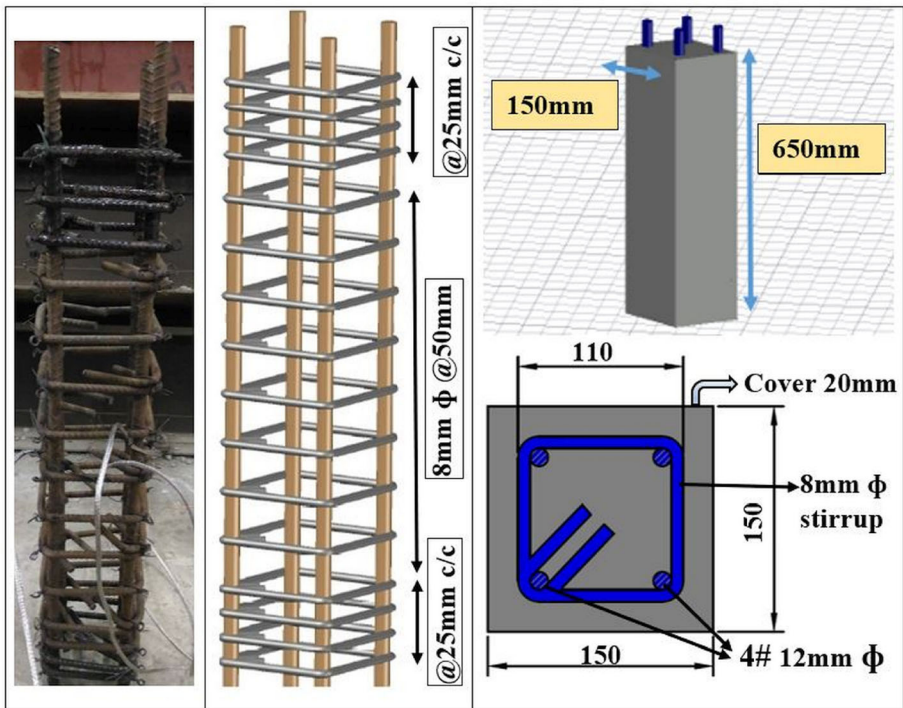


**Figure 1. Details of the column specimens (All dimensions are in mm).**

sure condition [44], using ordinary Portland Cement of 43-grade, fine aggregate conforming to zone-II, crushed limestone coarse aggregate of maximum nominal size 12.5 mm and tap water. Water to cement ratio of 0.5 was maintained in the mix design. The physical properties of the cement, fine aggregate and coarse aggregate are tabulated in Tables 3, 4, 5, 6, 7, following respective Indian standard codes [46, 47]. The average slump of the concrete mix was 75 mm. Hot rolled Tata Tiscon TMT steel reinforcements of 12 mm and 8 mm diameters were employed in all specimens. The measured yield and tensile strengths of the rebars are produced in Table 2. Rotating drum mixer and needle vibrator were used to cast the column specimens. Total six number of companion cubes of 150 mm side were cast for each batch of three columns. The column specimens and cubes were submerged in a freshwater tank for curing for 28 days. The average cube compressive strength of concrete after 28 days of curing was 37.56 MPa. IS 516 [48] was followed to test the cube compressive strength. Post 28 days of curing, the column specimens not to be corroded were kept in ambient air conditions inside laboratory. The specimens to be corroded on the other hand were kept for the desired duration in water tanks for accelerated corrosion regime, before taking them out and placing in ambient air conditions in the laboratory.

**Table 1**  
**Concrete Mix Proportions**

Ingredients	Cement	Water	Fine aggregate	Coarse aggregate
Mix proportion (kg/m <sup>3</sup> )	380	190	885	945

**Table 2**  
**Characteristics of Steel Reinforcement Bars (as Measured in the Laboratory)**

Nominal Diameter (mm)	Yield Strength (MPa)	Ultimate Strength (MPa)	Elastic Modulus (GPa)
8	488.5	585	200
12	490	598	200

**Table 3**  
**Physical Properties of Cement**

Properties	Obtained Results	Recommended values in IS 8112:2013	Units
Specific gravity	3.15	–	–
Blaine's fineness	310	225 (minimum)	m <sup>2</sup> /kg
Soundness Le Chatelier test	2.1	10 (maximum)	mm
Autoclave expansion	0.1	0.8 (maximum)	%
Normal consistency	29	30	%
Initial Setting Time	95	30 (minimum)	Minutes
Final Setting Time	178	600 (maximum)	
Compressive strength 28 days	45.62	43	MPa

**Table 4**  
**Physical Properties of Fine Aggregate**

Characteristics	Requirements per IS 383: 2016	Obtained results
Grading	–	Conforming to grading Zone-II
Fineness modulus	2.0 to 3.5	2.54
Specific gravity	2.6 to 2.7	2.62
Density (loose) (kN/mm <sup>3</sup> )		13.9
Moisture content (%)	–	0.47



**Table 5**  
**Sieve Analysis of Fine Aggregate as per IS 383:2016**

IS Sieve designation	Weight retained (gm)	Percentage weight retained	Cumulative % of weight retained	Cumulative % Weight Passing	% Passing for grading zone-II IS 383:2016
4.75 mm	12	1.2	1.2	98.8	90–100
2.36 mm	130	13	14.2	85.8	75–100
1.18 mm	179	17.9	32.1	67.9	55–90
600 $\mu$	220	22	54.1	45.9	35–59
300 $\mu$	332	33.2	87.3	12.7	8–30
150 $\mu$	117	11.7	99	1	0–10
Residue	10	1	100	–	–

**Table 6**  
**Physical Properties of Coarse Aggregate**

Characteristics	Requirements per IS 383: 2016	Obtained results
Fineness modulus	5.5 to 8	7.22
Specific gravity	2.6 to 2.7	2.64
Density (loose), kN/m <sup>3</sup>	–	15.6
Water absorption (%)	–	0.67
Moisture content (%)	–	Nil

**Table 7**  
**Sieve Analysis of Coarse Aggregate as per IS 383:2016**

IS Sieve Designation	Weight retained (grams)	Percentage of weight retained (%)	Cumulative percentage of weight retained (%)	Percentage of weight passing (%)	Range specified for 12.5 mm downgraded coarse aggregate per IS 383:2016
16 mm	0	0	0	100	–
12.5 mm	370	7.4	7.4	92.6	90–100
10 mm	730	14.6	22	78	40–85
4.75 mm	3860	77.2	99.2	0.8	0–10
2.36 mm	25	0.5	99.7	0.3	–
Residue	15	0.3	100	–	–

The column specimens were cast and tested in triplicate and test results produced were average of three samples. The experimental variables included were the degree of corrosion and the exposure temperature. The nomenclature of the specimens were designated by two numerals and a letter. The first letter C stands for column specimen. The second numeral represents the degree of corrosion spec-

**Table 8**  
**Test Matrix**

Designation of column	Temperature (°C)	Corrosion Degree (%)	No. of Specimens
C-0-0	0	0	3
C-0-5	500	0	3
C-0-8	800	0	3
C-10-5	500	10	3
C-10-8	800	10	3
C-20-5	500	20	3
C-20-8	800	20	3

imen is subjected to (0, 10 and 20 for 0%, 10% and 20% degree of corrosion respectively). The third numeral stands for the temperature of exposure (0 for ambient temperature, 5 for 500°C and 8 for 800°C). Table 8 shows the test matrix for the experimental investigation.

### 3.2. Accelerated Corrosion Test

To determine the adverse effects of corrosion within a realistic timeframe it is essential to expedite the corrosion process in the laboratory. Various accelerated chloride-induced corrosion techniques have been developed to significantly reduce the time taken for corrosion initiation. Impressed current technique was followed in present investigation to corrode the concrete specimens. The column specimens were immersed in a tank with saline solution of 3.5% sodium chloride (NaCl), to simulate corrosive environment as shown in Fig. 2. Thin stainless-steel plates were cut to appropriate size and attached at the mid-height in test length portion of each surface of the columns. A schematic diagram of electrical connections set up for the process is shown in Fig. 2. A specially designed DC supply (current control/voltage control) of 30 Ampere and 100 Volt capacity was employed for applying accelerated corrosion. The negative terminal of output DC supply was connected with stainless steel plates that acted as the cathode and the positive terminal of the output DC was connected to embedded reinforced steel bars acting as the anode. Specimens were subjected to corrosion exposure after 60 days of age. Constant corrosion current density of 200  $\mu\text{A}/\text{cm}^2$  was supplied throughout the exposure duration, which is about twenty times the corrosion intensity observed in severely corroding RC structures [11]. DC voltage and DC current values in all specimens were recorded after every 24 h interval.

The degree of corrosion (DOC) (Eq. 1) is defined as the ratio of weight of steel consumed to the original weight ( $W_0$ ) of the steel bar, expressed in percentage.

$$\text{DOC}(\%) = \frac{W_0 - W_f}{W_0} \times 100 \quad (1)$$

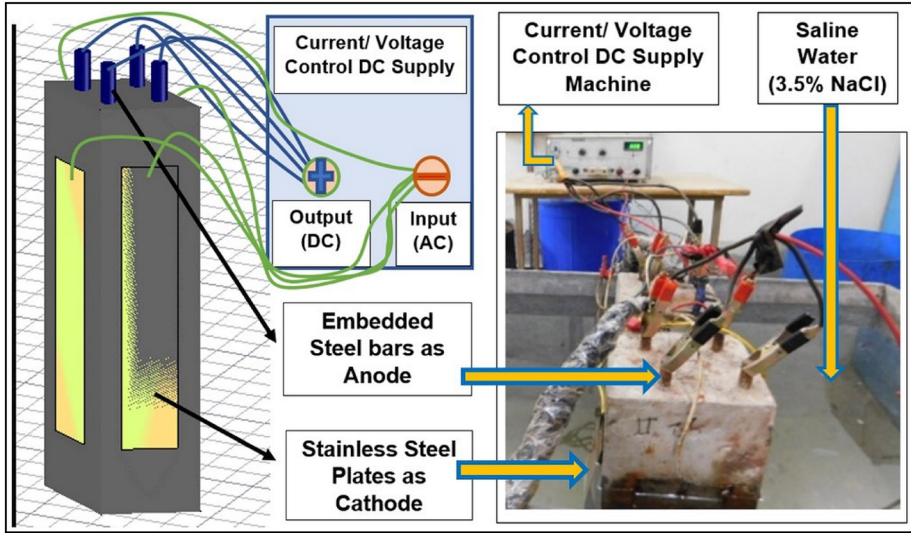


**Figure 2. Accelerated corrosion test set-up.**

where,  $W_0$  = Original weight of non-corroded steel bar,  $W_f$  = Final weight of steel bar after target level of corrosion. The electrical energy consumed determines the amount of corrosion, which is a function of the current supplied, potential difference, and time interval. Keeping the current density constant at  $200\mu\text{A}/\text{cm}^2$ , the total amount of charge required to achieve target degree of corrosion was estimated by incorporating Faraday's law (Eq. 2) which states:

$$\Delta m = \frac{M.I.t}{Z.C_{Faraday}} \quad (2)$$

where  $\Delta m$  = mass of steel consumed,  $M$  = Molar mass of iron = 55.84 mol,  $I$  = Electric Current in Amperes,  $t$  = time in seconds,  $Z$  = number of electrons liberated in anodic reaction, ionic charge equal to 2;  $C_{Faraday}$  = Faraday's constant equals to  $96,500 \text{ C mol}^{-1}$ .

In order to account for the presence of concrete and different environment condition in laboratory test conditions, a correction factor  $\lambda$  was considered to calculate the required duration of exposure (Eq. 3). Based on previous studies [21] the value of  $\lambda$  was taken equal to 1.5.

$$t = \frac{\lambda.\Delta m.Z.C_{Faraday}}{M.I} \quad (3)$$

The designed values of current and duration of exposure are given in Table 9.

Considering the limited number of specimens to be tested, two different levels of corrosion were chosen. To observe a significant effect of corrosion on the residual compressive strength of the heated columns, a minimum of 10% degree of corro-

**Table 9**  
**Designed Accelerated Corrosion Details**

Degree of corrosion (%)	Mass loss per column (gm)	Current (A)	Duration (days)
10	371.47	0.404	55
20	742.94	0.404	110

sion was chosen. Furthermore, RC columns with corrosion level more than 20% are considered damaged and retrofitting is generally recommended [49]. There was limitation on the time frame considered for the experimental program as well. Higher the degree of corrosion targeted, higher the duration required to achieve it. Hence the maximum level of corrosion was chosen to be 20%.

### 3.3. Thermal Testing

Subsequent to completion of corrosion process, the columns were exposed to the designed heating and cooling regime in a vertical split type high temperature electrical furnace. The exterior of the furnace was octagonal, it had an inner compartment with 210 mm diameter and 450 mm height. It could accommodate a single specimen at a time. The specimen in the test length of 450 mm was kept inside the furnace. The 100 mm lengths at both ends were protruding out of the furnace, it was fully sealed with glass wool, insulating the column test length. The programmable electric furnace had a maximum heating capacity up to temperature of 1000°C and had an accuracy of 1°C. The furnace was controlled by microprocessor-based temperature controller with ‘K’ type thermocouples provided in the furnace chamber. Figure 3 shows a view of the complete setup of column with electrical furnace. All uncorroded and corroded column specimens underwent the same thermal exposure program. K-type chromel–alumel thermocouples, were fixed at mid-heights in the columns during casting, at two locations in the cross section: at the centre of the column and at the cover-core interface. For measurement of surface temperature, one thermocouple was placed inside the furnace. The columns were heated in the furnace to the target temperatures of 500°C and 800°C. The constraints of limited number of specimens led to design only two levels of target temperatures for the current experimental study. The minimum level of temperature to show some significant results in residual compressive strength degradation of columns, was chosen to be 500°C. In the context of simplified calculation for 500°C isotherm method in Annex B of Eurocode 2 [50], 500°C is assumed as the limiting temperature for concrete section contributing to the load bearing capacity of the RC member. 500°C is a level chosen in the Eurocode [50] to determine cross sectional areas, which may be assumed to be unaffected by high temperature exposure. However, even though temperatures in the remaining cross section may be considered lower than 500°C, rebar temperatures and corrosion of rebars, may still have significant impact on the residual strength of the RC member. Arguably, the chosen 500°C level of heating, is a level to verify the impact of the Eurocode



**Figure 3. Furnace set-up.**

assumption, if and when corrosion takes place. Previous studies show that during a fire scenario the maximum temperature usually falls in the range of 1000°C to 1200°C. However, usually high temperatures in this range primarily occur at the surface of the RC structures and they are hardly sustained as they are subject to pronounced fluctuations [51]. The pre-existing corrosion in the columns was the factor considered while choosing the heat exposure program. As the topic is at a nascent stage, with limitations on the number of specimens, the highest level of heat exposure was designed at 800°C. This was so as not to cause a damage so severe to the columns, that it would be difficult to record the proper load–deflection behaviour, including the post-peak section of the curve, during axial compressive strength test. Thus, target temperatures of 500°C and 800°C are reasonable for current investigation. The heating rate maintained for all specimens was 10°C/minute as per the capacity of the electric furnace. Since prior to heat exposure the columns were damaged by corrosion, to maintain integrity of the specimens during mechanical testing, the target temperature was maintained for one hour. The thermocouples were connected to the data acquisition system to record the time–temperature data inside the specimen and furnace. The columns naturally cooled down to ambient temperature after the designed heat exposure program was completed, the cooling rate was not controlled. The time–temperature history during whole heating and cooling cycle was recorded. Given the exploratory nature and available resources, the elevated temperature exposure is taken artificially, and not related to standard fire heating, which is a recommended step for further research

work. After 7 days of cooling in room temperature, the columns were taken for uniaxial compression test.

### **3.4. Residual Mechanical Testing**

Following the completion of designed heating and cooling regime, axial compression test of the specimens was carried out. The column specimens were tested using HEICO automatic servo-controlled compression testing machine with a capacity of 5000 kN, with displacement control capabilities (Fig. 4). A rate of 0.1 mm/minute was chosen for the monotonic concentric compression load to register the post peak response of columns properly. To prevent premature failure at the ends, external confinements were provided by fixing steel collars of 20 mm thickness and 100 mm length at the top and the bottom ends of the column. Failure of the column was designed to be in the test region of 450 mm in the middle section of the specimen. Two linear variable differential transducers (LVDTs) were employed to measure the axial contraction of the column specimens. They were attached at opposite sides of the square column using steel clamps along the gauge length of 300 mm. The average of the two deflections measured by the LVDTs was taken as the mean axial displacement of the centroidal section of the column. The inbuilt load cell in the HEICO instrument recorded the load values. The data from the load cell and LVDTs were registered into a data acquisition system.

## **4. Observations During Testing**

### **4.1. Observations After Accelerated Corrosion Test**

Twelve column specimens were tested under accelerated corrosion process with a current density of  $200 \mu\text{A}/\text{cm}^2$ . After the exposure for required duration, the surfaces of the corroded specimens were thoroughly cleaned for the proper inspection of surface cracks. Crack widths were noted down using crack scope of least count 0.05 mm. The crack positions were also noted along the length and breadth of the surfaces, using a measuring tape, noting down the x and y coordinates of the cracks. Cracks orientations showed that cracks developed along all directions. Whereas majority of it was along longitudinal direction, cracks developed along diagonal directions as well. The crack locations were spread along the entire surface since all the longitudinal and transverse reinforcement bars were corroded simultaneously. Rajput et al. [22] observed that the orientation of reinforcing bars being corroded affect the direction of corrosion cracks. Most of the previous studies [18, 21] observed cracks developed only along a specific direction as they examined the effects of corrosion on only longitudinal bars or only transverse bars. Present study has targeted corrosion in the whole reinforcement cage, which is observed in ageing RC structures facing durability issues. The crack distributions over all four surfaces are shown in Fig. 5. The crack widths varied from 0.05 mm to 1.2 mm in samples with 10% corrosion degree. Severity of corrosion induced distress increased further in samples with 20% corrosion degree, the crack

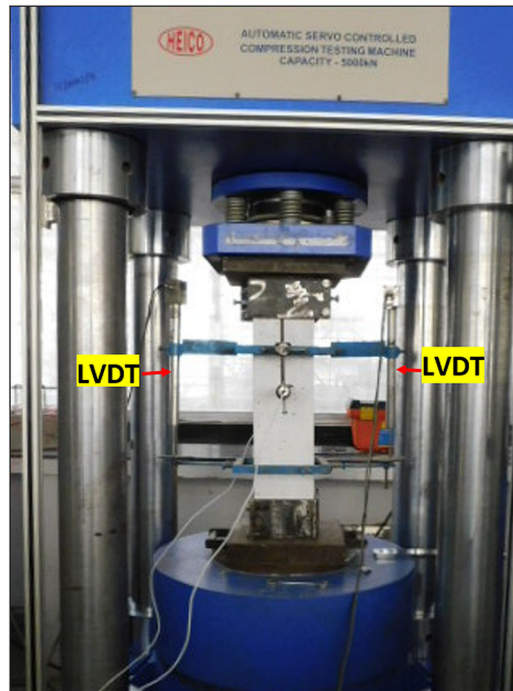
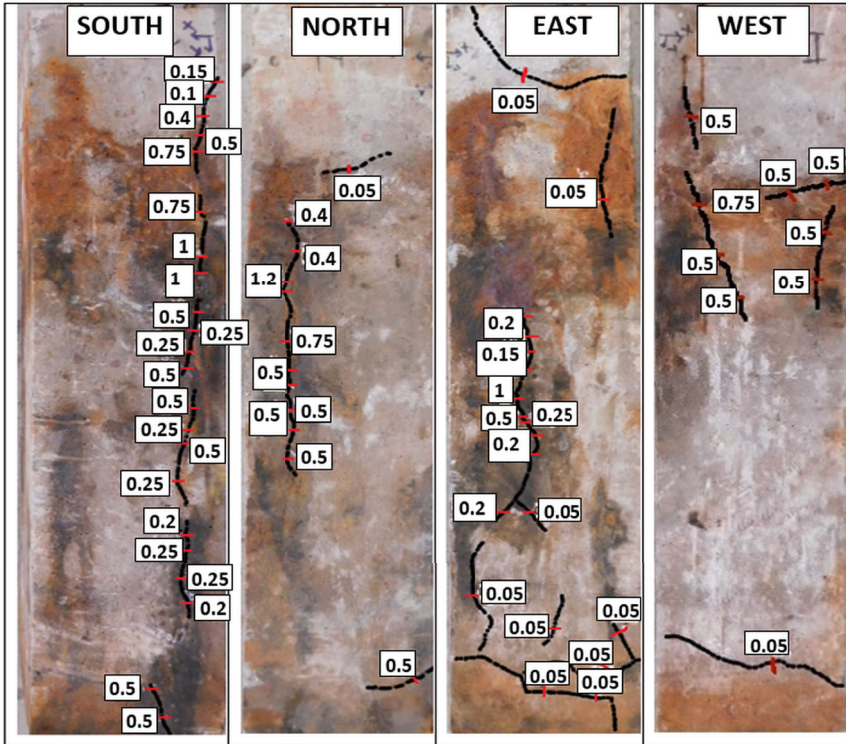
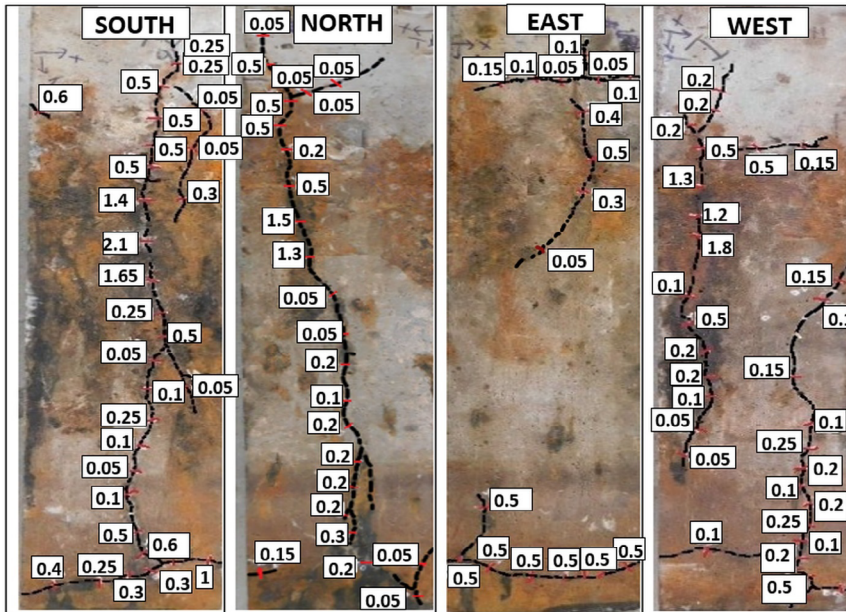


**Figure 4. Uniaxial compression test setup.**

widths varied from 0.05 mm to 2.1 mm. Although all samples had similar reinforcement configuration, with same materials being used to cast the specimens, further they were exposed to similar conditions in accelerated corrosion set-up, still the crack patterns were not uniform along all four surfaces of the columns. In Fig. 5a, the crack widths varied from 0.05 mm to 1.2 mm for South, North and East face, whereas West face had relatively lesser corrosion distress in terms of surface cracks and maximum crack width was 0.75 mm. Further as per Fig. 5b three faces of South, North and West showed more surface cracks with widths varying from 0.05 mm to 2.1 mm, whereas East face had relatively lesser cracks with maximum crack width being 0.5 mm. It may be due to the difference in resistance each face provided, which can be attributed to the non-uniformity of microstructure of reinforced concrete and variations with progression of corrosion process. Corrosion leads to dissolution of steel, resulting in loss in cross section of the bar. It generates expansive corrosion products, that generate internal stress on concrete. When the tensile strength of concrete is exceeded by these internal stresses, micro cracking starts in the surrounding concrete and cracks eventually appear on the external surface of structural element. If availability of oxygen at the anodic site is insufficient, the ferrous ion will stay in concrete pore solution or get transported and deposit elsewhere in pores and microcracks in the concrete, which results in significant loss in section without the distress caution given by concrete cracking or spalling [49]. Hence cracks may form away from anodic sites



(a) Column with 10% corrosion



(b) Column with 20% corrosion



**◀Figure 5. Corrosion induced crack patterns (mm) in column with (a) 10% corrosion (b) 20% corrosion.**

where actual corrosion takes place, depending on the location of deposition of corrosion products.

#### **4.2. Observations After Thermal Exposure**

*4.2.1. Crack Pattern After Thermal Exposure* Visual observations of crack patterns on column surfaces after thermal exposure was carefully assessed. As discussed earlier, surface cracks developed in columns post corrosion. Further subjecting those corroded columns to elevated temperature conditions in the furnace, resulted in formation and propagation of more surface cracks. The differential strains between the cement paste and aggregate due to rising temperature and thermal gradient inside concrete, give rise to tensile stress that can cause cracks in concrete [52]. The dehydration of the C-S-H gel and the thermal expansion of the aggregate generate internal stresses, temperatures exceeding 300°C induce microcracks in the concrete. In the temperature range of 400°C to 600°C the crystals of calcium hydroxide break down forming calcium oxide and water. During the cooling phase the calcium oxide absorbs water from the ambient air which results in expansion with formation of calcium hydroxide, leading to widening of the cracks [53].

Crack lengths were higher in specimens subjected to higher temperature of exposure as well as higher degree corrosion. For non-corroded specimens subjected to elevated temperature, C-0-8 had larger in length and more pronounced cracks than C-0-5, all crack widths being 0.05 mm. Although cracks formed in all directions, significant amount of cracks formed along transverse direction. It might be due to the fact that transverse reinforcements are closest to the surface. When heat is applied to the surface, thermal gradient starts affecting the surrounding area of the transverse reinforcement first, near the steel-concrete interface, forming microcracks in the concrete.

For corroded columns, as the temperature of exposure increased, the thermal cracks increased. Majority of the new cracks developed due to thermal exposure had crack width of 0.05 mm. The thermal cracks were seen to be forming along pre-existing corrosion cracks, joining those crack lines. It can be possibly due to pre-existing microcracks along those lines grow due to thermal stress and form visible cracks on surface after heat exposure. As the concrete surrounding those crack lines are more vulnerable to further crack propagation. Also new thermal cracks formed along transverse direction in all specimens, along a length of 90 mm to 140 mm on each face. It might be explained as the stirrups are located closest to the column surface, they are the most damaged after accelerated corrosion test, in addition they are exposed to the heat for a longer period compared to parts further towards the core of the column. The concrete surrounding the corroded stirrup is particularly vulnerable to cracks formation. Thus, rise in thermal

gradient causes generation of cracks along the stirrups, forming cracks along the transverse direction.

*4.2.2. Time–Temperature History Analysis* Thermocouples were embedded inside the columns and positioned inside the furnace to track the thermal history throughout the heating and cooling regime. The thermal responses of each specimen were then investigated by plotting the time–temperature curves. The average representative curves of the columns are illustrated in Figs. 6a–f.

Due to low thermal diffusivity of concrete, the increase in temperature in the deeper layers is a slow process. In case of fire events in RC structures, the uneven temperature distribution leads to hotter outer surface and relatively cooler inner core. It leads to rise in thermal gradients in the structure. The magnitude of thermal gradients developed depend on the fire intensity and its duration, the size and shape of RC elements and their material properties etc. Thermal gradients can result in differential strains within the concrete. These temperature-induced stresses can lead to tensile stresses that increase the risk of cracking in the concrete [51–53]. As can be seen in the Figs. 6a–f, the rate of temperature rise was higher at the surface of the specimens as compared to at the centre. Further, the time–temperature curves showed perturbations in the concrete temperatures between 100°C and 200°C. This temperature range corresponds to the release of free water and subsequently chemically bound water in concrete [54]. A moisture front is driven by the heat toward the central region of the specimen, decreasing the escalating rate of temperature there. It led to higher thermal gradient between the surface and the centroidal region of the specimen. It was also observed that for the specimens subjected to the same temperature of exposure (Figs. 7a and b), the value of maximum temperature at the centre ( $c1_{max}$ ) was decreasing with rising degree of corrosion. E.g., for specimens subjected to 500°C, the value of maximum temperature at centre was 329°C for non-corroded sample, while it was 316°C for 10% corroded sample, and 292°C for 20% corroded sample. Similarly for specimens subjected to 800°C, the value of maximum temperature at centre for non-corroded specimen was 609°C, while it was 591°C for sample with 10% corrosion and for sample with 20% corrosion degree it was 557°C. Also, it was noticed that the difference in the time of attainment of the  $c1_{max}$  and the time at which furnace cooling starts, decreases with increasing corrosion degree. While for C-0-5 it was 121 min, for C-10-5 it was 116 min and for C-20-5 it was 112 min, with cooling starting from 110 min. Similarly for C-0-8 it was 166 min, while for C-10-8 it was 158 min and for C-20-8 it was 151, with cooling starting from 141 min. As the maximum temperature at centre was attained after cooling began, so the sound specimens were able to retain the temperature for a longer duration as compared to corroded samples. Due to pre-existing cracks in corroded samples, the heat flow might be happening in radial direction, making it difficult for corroded specimens to retain the temperature for long after cooling started. Further research is recommended to study the heat transfer mechanism extensively in corroded RC columns.

The difference between surface and centre temperature was plotted to study the thermal gradients in the specimen throughout the heating and cooling excursions.

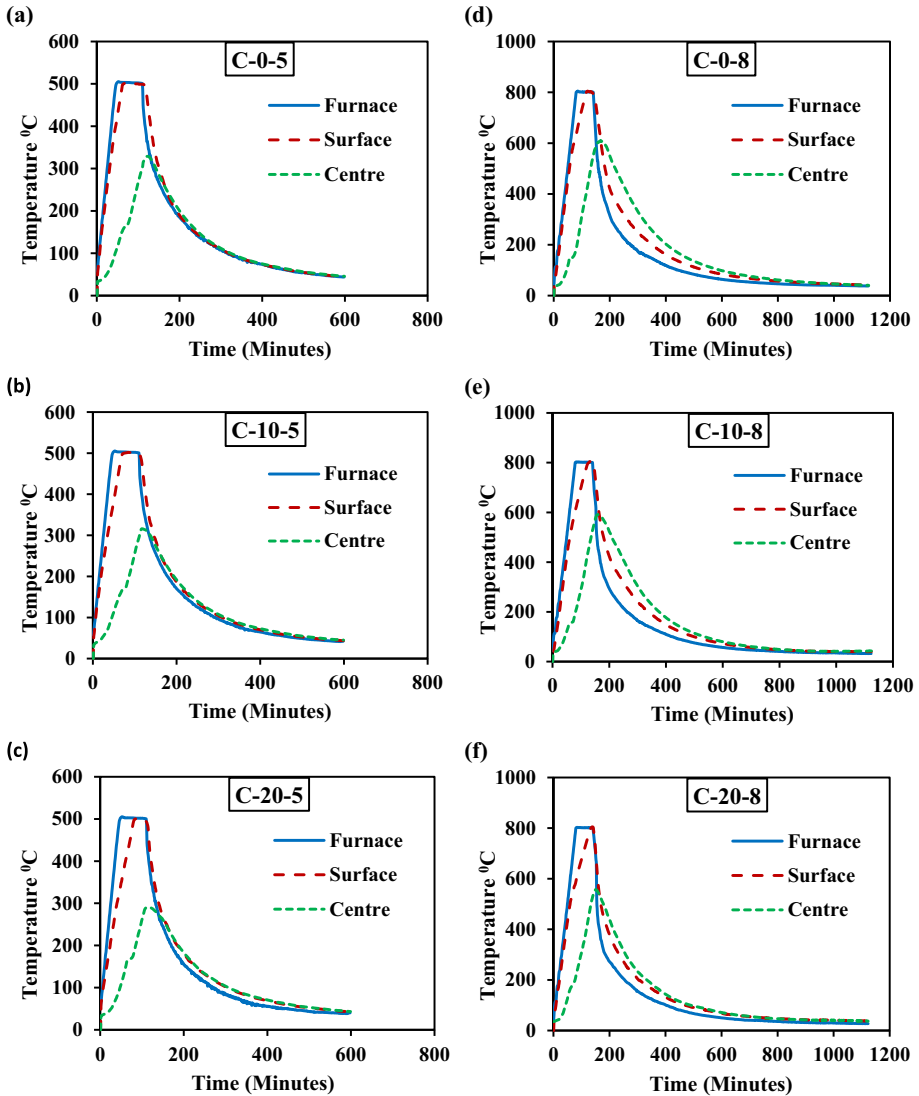


**Figure 6. Time-Temperature curves for columns: (a) C-0-5; (b) C-10-5; (c) C-20-5; (d) C-0-8; (e) C-10-8; and (f) C-20-8.**

The maximum and minimum value of temperature difference between centre and surface, time corresponding to those points, the respective maximum and minimum thermal gradients, surface temperature corresponding to those points, are compiled in the Table 10. Figures 8a & c show the variation of difference in temperature between surface and centre ( $\Delta T$ ) with time. The figures indicate that  $\Delta T$  increased to reach a maximum positive value in the beginning, afterwards it decreased to get to a maximum negative value, reaching ambient temperature at

the end. For better visual representation of thermal gradients, the values of temperatures at the two locations, i.e., at the centre and surface of the columns are plotted, corresponding to different times with 40 min intervals, as shown in Fig. 8b and d. Temperatures at the two locations at 40, 80, 120 and 160 min are presented in Fig. 8d. The time till the initiation of cooling of furnace was considered for the plots.

The results indicate that the maximum positive thermal gradient increases with increasing temperature of exposure regardless of degree of corrosion. However, more the degree of corrosion, lesser is the value of maximum thermal gradient for the same temperature exposure. While the maximum temperature difference between surface and centre for samples exposed to 500°C was 345°C for non-corroded specimen, it was 330°C for 10% corroded, 315°C for 20% corroded sample. Furthermore, for samples exposed to 800°C, the value was 451°C for non-corroded specimen, 414°C for sample with 10% corrosion degree, and 381°C for sample with 20% corrosion degree. The value of maximum positive thermal gradient decreased as the degree of corrosion increased. The presence of microcracks, the increased porosity due to corrosion may aid in radial thermal flow inside corroded columns. Also, more the temperature of exposure, more was the difference between the thermal gradients between non corroded and corroded samples. While the difference was 4°C/cm between C-0-5 and C-20-5, it was 11°C/cm between C-0-8 and C-20-8. Also, the time of attainment of the maximum thermal gradient was higher for more corroded specimens. It was 61 min, 70 min, and 80 min for C-0-5, C-10-5, and C-20-5, respectively; while it was 76 min, 85 min and 90 min for C-0-8, C-10-8, and C-20-8, respectively. It can be attributed to the presence of pre-existing cracks in corroded specimens allowing heat flow through the specimens.

The results further reveal that the maximum positive thermal gradient correspond to higher surface temperatures in more corroded specimens. In the cooling stage, the magnitude of maximum negative thermal gradients were much smaller compared to the corresponding maximum positive thermal gradient. More the temperature exposure, more was the magnitude of cooling gradient. The cooling gradient for columns exposed to 500°C were -1.5, -1 and -0.7°C/cm for samples with 0%, 10% and 20% corrosion. While cooling gradient for columns exposed to 800°C were -17.4, -14 and -8.6°C/cm. The presence of cracks in corroded samples might have been accelerating the cooling process. Since the heat exposure program was of limited duration, along with other constraints such as functionality of the electric furnace available, and the number of specimens tested, further research is recommended to investigate the heat transfer mechanism in corroded columns to draw relevant conclusions.

### **4.3. Ultrasonic Pulse Velocity Testing**

Damage assessment of the RC columns was carried out by ultrasonic pulse velocity (UPV) test. UPV testing is among the various non-destructive test methods that is used to determine the level of damage in the concrete. It incorporates the measurement of velocity of sound in its design mechanism. Velocity of sound in concrete is a credible indicator of thermal damage as it is sensitive to any change

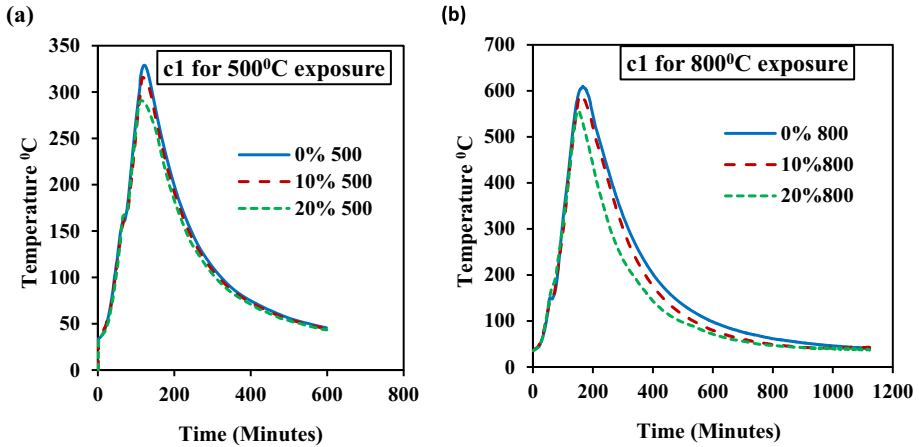


**Figure 7. Time-temperature curves at the centre of the columns exposed to temperature of (a) 500°C and (b) 800°C.**

**Table 10  
Temperature Histories of Columns**

Columns	Maximum Temperature difference $\Delta T$ (°C)		Maximum Thermal Gradient (°C/cm)		Time at maximum thermal gradient (minutes)		Surface Temperature at max gradient (°C)		c1 max (°C)	Time at c1 max (minutes)
	+ ve	-ve	+ ve	-ve	+ ve	-ve	+ ve	-ve		
C-0-5	345.5	-11.0	46.1	-1.5	61	183	497.6	213.2	328.9	121
C-10-5	330.4	-7.5	44.1	-1.0	70	211	498.6	169.4	316.0	116
C-20-5	315.0	-5.2	42.0	-0.7	80	211	497.8	163.9	291.0	112
C-0-8	451.1	-130.9	60.1	-17.5	76	202	622.3	411.0	609.5	166
C-10-8	413.9	-105.2	55.2	-14.0	85	204	633.9	407.9	591.4	158
C-20-8	381.1	-64.8	50.8	-8.6	90	203	641.7	367.0	557.0	151

in Young's modulus [55]. The decomposition of the cement paste and dehydration of CSH gel, along with the thermal incompatibility between aggregate and cement paste, leads to inferior concrete mechanical properties as heating progresses. Moreover, the process of moisture expulsion due to dehydration affects the velocity of sound. The process of corrosion also degrades the mechanical properties of concrete. To assess the damage to the columns after corrosion and after thermal exposure, UPV test was conducted in two steps. Once after the completion of accelerated corrosion process, then a second time following the complete cycle of heat exposure program. The transmitting and receiving transducers were placed on the opposite surfaces of the columns and were pressed firmly against the col-

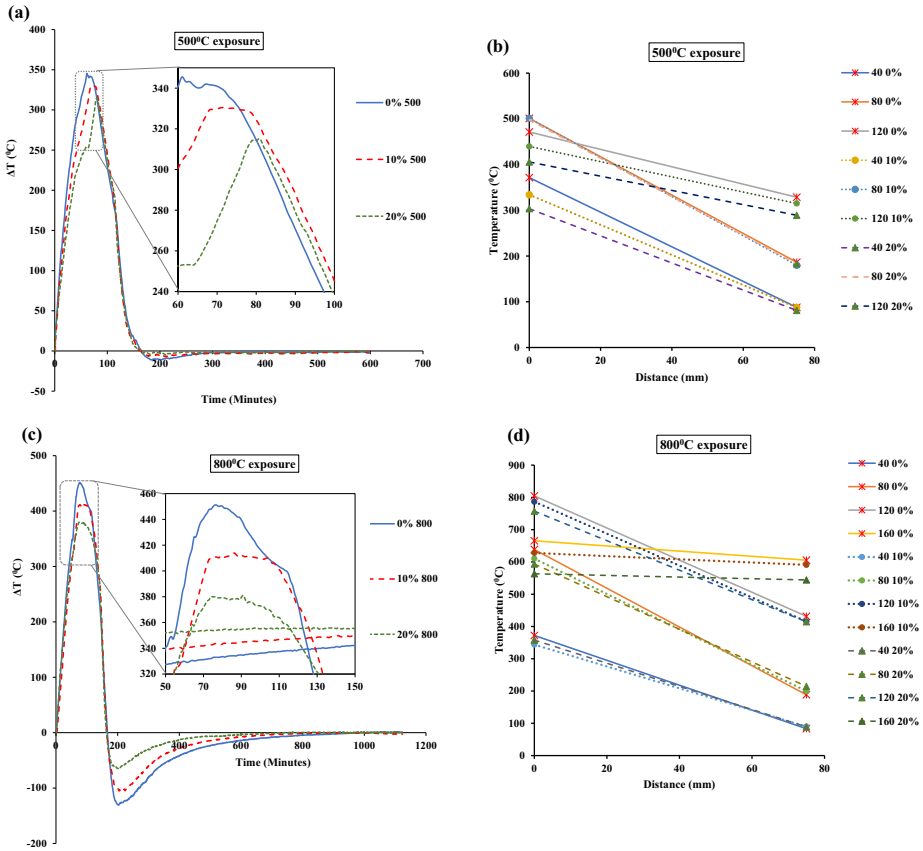


**Figure 8. Plots for thermal gradients in columns. (a) & (c): Plots of difference in temperature between surface and centre vs time for columns exposed to temperatures of 500 °C and 800 °C respectively. (b) & (d): Plots of temperatures at two locations. i.e., at centre and surface, at 40 min intervals (at 40, 80, 120 min), for columns exposed to temperatures of 500 °C and 800 °C respectively.**

umn surfaces until a constant reading was observed. The pulse velocity through the concrete was calculated by dividing the distance between the transducers with the transit time displayed. The UPV values at the centre of the column specimens were taken. Average UPV value of three specimens for each series is reported. The average UPV test results were plotted as shown in Fig. 9.

**4.4. Observations from Crack Development After Mechanical Loading**

The details of crack propagation in columns, i.e., the location of the cracks along the surfaces in the gauge length of 300 mm and the corresponding load during the crack generation were noted down as the axial compression testing progressed. For better visual representation, diagrams were drawn (Figs. 10a–f) to clearly

illustrate the locations of the cracks developed on the surface of the columns in every step. The names designated for four faces of the columns were East(E), West(W), North(N) and South(S). Full-length column is represented in the diagram to showcase corrosion cracks with solid green lines and thermal cracks with dotted orange lines. Corresponding diagram of crack details during axial compressive testing in gauge length of 300 mm is shown next to it. The crack lines are shown in solid blue lines along with corresponding load (kN) at the moment of initiation of the cracks.

For non-corroded specimens, it can be observed from the diagrams that cracks during compressive test formed along the lines of pre-existing cracks in the columns, e.g., in Fig. 10b C-0-8 on the East & South face, the crack propagation during compressive test is mirror image of pre-existing cracks. The crack initiation load was 440 kN for C-0-5 and 390 kN for C-0-8.

The crack propagation during compressive test was majorly influenced by the already existing crack patterns in the columns. Possible explanation might be that these pre-existing crack lines provide the path of least resistance for the crack propagation during axial loading. The compressive load for crack initiation for C-10-5 & C-10-8 was 300 kN and 220 kN respectively. Whereas for C-20-5 & C-20-8 it was 110 kN & 100 kN respectively. The results indicate that the crack initiation load depends primarily on the degree of corrosion as compared to the temperature of exposure. The crack initiation load for C-10-5 & C-20-5 reduced by 31.8% & 75% of that for C-0-5. For columns C-10-8 & C-20-8, the crack initiation load reduced by 43.5% and 74.35% of corresponding value for C-0-8. The crack initiation load for C-20-5 reduced by 66.66% of that for C-10-5 and for C-20-8 reduced by 54.54% of the same for C-10-8. Thus, with temperature of exposure remaining the same, the degree of corrosion affects the crack initiation load significantly. Whereas crack initiation load for C-10-8 reduced by 26.65% of that for C-10-5 and the same for C-20-8 reduced by 10% of corresponding value for C-20-5. The influence of temperature of exposure on crack initiation load is seen to decline with rise in corrosion damage to the columns.

Most initial cracks were observed to be forming along the transverse direction during mechanical testing. As the load increased, the cracks started forming along the longitudinal direction. However, in columns with 20% degree of corrosion, the initial cracks started forming along longitudinal direction as well. It was also observed that for the same exposure temperature, extent of new cracks formed after heating in furnace was lower in columns with higher degree of corrosion.

#### **4.5. Observations from Corrosion Damage**

After axial compressive test was over, columns were taken out and demolished. Figures 11a & b shows the visuals of the columns before demolition, cover concrete was removed, and visual inspection of the corroded reinforcement was carried out. It can be seen from Fig. 11 that both longitudinal bars and stirrups suffered considerable damage due to corrosion. Severe pitting corrosion was seen along the longitudinal and transverse bars at some locations. Column with 10% corrosion shows moderate damage to stirrups and longitudinal bars. Some of the

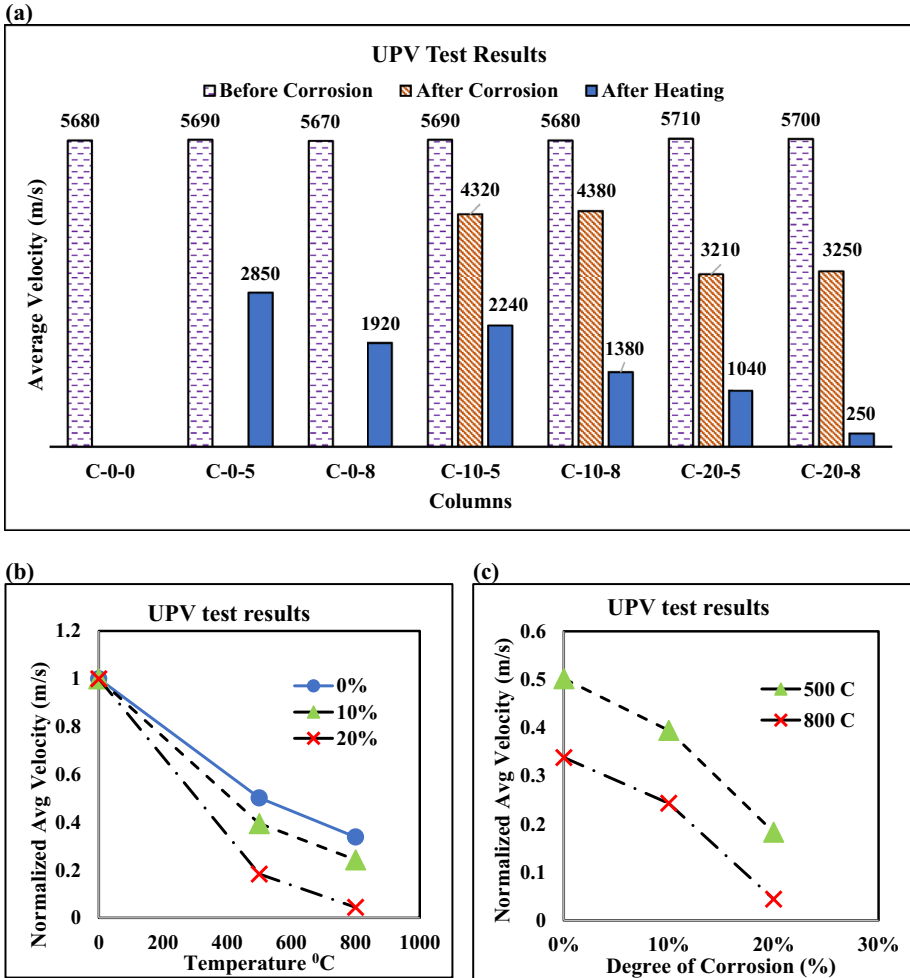


**Figure 9. UPV Test Results (m/s) of all columns; Variation of normalized UPV values with (b) temperature (c) degree of corrosion.**

transverse bars suffered more than 60% loss of cross section at the corner in some locations. In column with 20% corrosion, some of the transverse reinforcements had complete loss of cross section at the corner and severe pitting corrosion along longitudinal bars. It resulted in lack of lateral support transverse reinforcement were supposed to provide to the column, they were deemed ineffective. This led to increase in unsupported length of longitudinal bars, which was already damaged by severe pitting, which eventually induced premature buckling and failure of column. All columns failed under compression mode.

Gravimetric examination of the corroded bars was conducted after visual inspection was over. The column specimens were demolished, the corroded reinforcement from the test length were extracted. As per the guidelines of ASTM:



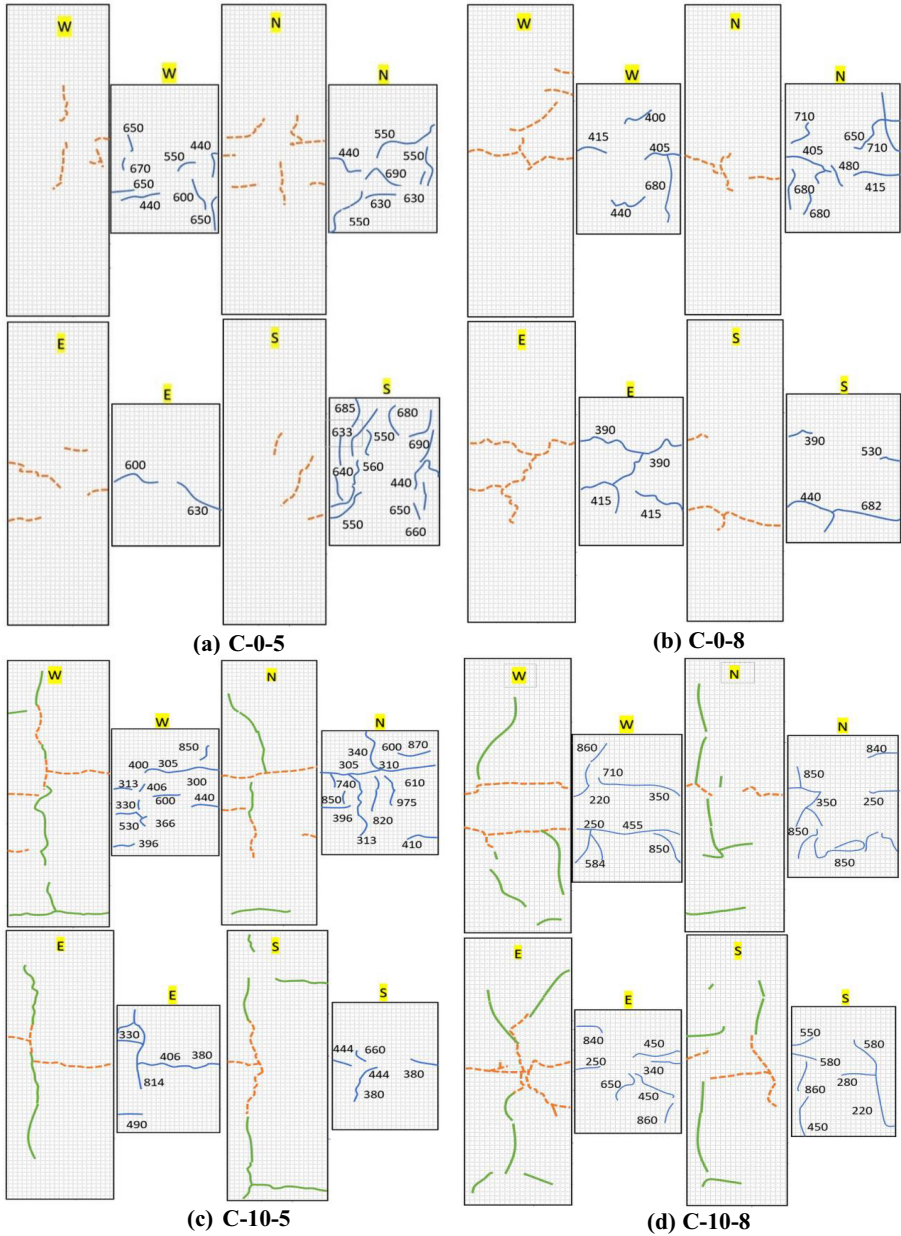


**Figure 10. Schematic crack pattern of columns (a) C-0-5; (b) C-0-8; (c) C-10-5; (d) C-10-8; (e) C-20-5; (f) C-20-8 (Load values are in kN).**

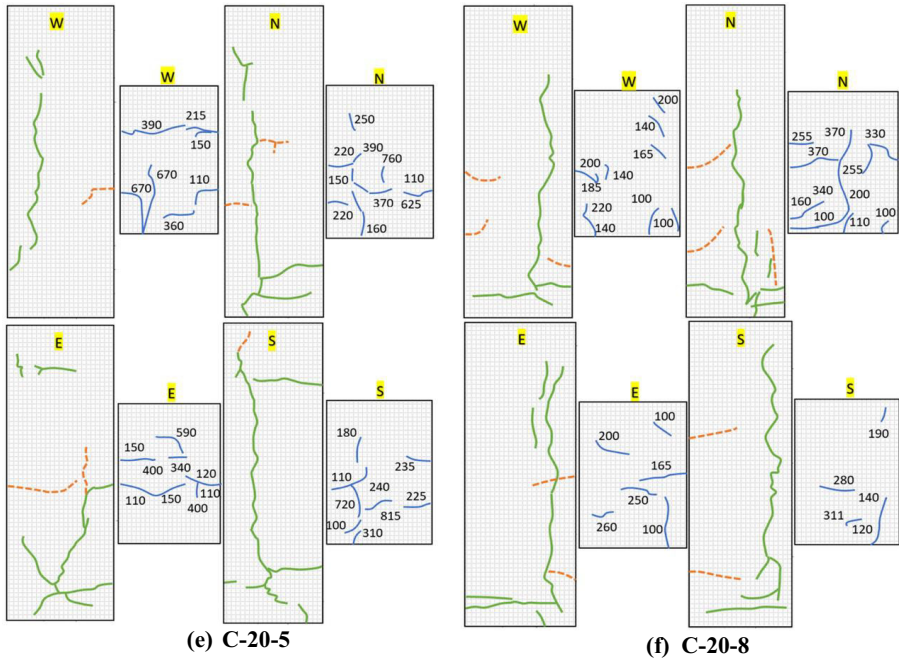


**Figure 10. continued.**

G1-03 [56], the reinforcement bars were cleaned with chemical and mechanical methods. The loss of weight of individual components was measured and reported in percentage as degree of corrosion. The average corrosion degree for each individual column was calculated by averaging mass loss of all elements. The columns that were targeted for 10% degree of corrosion had an average corrosion degree of 8.78%, with longitudinal bars suffering mass loss of 6.65% and transverse reinforcement having an average corrosion percentage of 10.39%. Different elements of the same column suffered different levels of damage. Individual stirrups corrosion level varied from 8.67% to 11.71%. For columns targeted for 20% degree of corrosion, average of 17.85% of corrosion was achieved, with longitudinal bars having an average corrosion percentage of 14.81%, whereas transverse bars suffered an average of 20.15% degree of corrosion. The corrosion degree of individual stirrups varied from 18.5% to 23.81%. It could be seen that transverse reinforcement suffered more level of corrosion compared to longitudinal bars. As stirrups are closest to the exterior surface of column, they are affected first due to their location during corrosion exposure. Furthermore, the bent corners of the stirrups create microcracks in the concrete surrounding them due to their geometry, making the columns vulnerable to further corrosion damage. It was observed that there was complete section loss at the corners of some of the stirrups. In all samples usually the corner of the stirrups were the most damaged parts due to corrosion. Even at 10% targeted corrosion degree, there was significant loss of



(a) 10% Corrosion



(b) 20% Corrosion

**Figure 11. Corrosion damage visuals of columns with corrosion (a) 10% (b) 20%. (a) 10% Corrosion. (b) 20% Corrosion.**

cross section in the stirrups. Thus, the functionality of stirrups for providing adequate confinement and shear strength to the column is compromised. In columns subjected to 20% degree of corrosion, some of the stirrups had part of the steel

completely consumed in the corrosion process at few locations, leaving it open-ended. It nullified the very purpose of the providing stirrups in the column. Pitting corrosion was observed along the longitudinal bars.

## 5. Analysis of Results

Typical load–displacement curves of columns after uniaxial compression test are presented in Figs. 12a–f. The results of the compression tests are summarized in Table 11. The initial load–displacement curves of all columns displayed linear behaviour irrespective of exposure conditions. More the extent of damage to the column, the shorter was the linear ascending portion of the curve. The linear ascending portion of the load vs displacement curve of control column was longer than that of all the columns exposed to heat and accelerated corrosion. It is well-established that an increase in cracks in concrete specimens results in non-linearity in load-deformation curves, which was the case with all columns subjected to elevated temperature and accelerated corrosion. Higher the degree of exposure, the more the damage to the column specimen, resulting in more cracks. Post-peak behaviour depended on the type of exposure as well, both on the degree of corrosion and the temperature of exposure. Higher the temperature of exposure of the column, flatter was the post-peak section of the load–displacement curves with higher rate of axial deformation, irrespective of the degree of corrosion suffered.

The slope of load–displacement curves in Fig. 12 clearly indicate that the stiffness of the columns decreases with increase in temperature of exposure. In comparison, degree of corrosion has much lesser influence on the stiffness of the columns. Thus, the temperature of exposure significantly affects the stiffness of the columns in comparison to the degree of corrosion.

For quantitative representation of ductility of RC columns, the ductility factor of columns was calculated. Ductility factor ( $\Delta$ ) is taken as the ratio of ultimate displacement to the yield displacement. Ultimate displacement is the post-peak deflection when load value drops to 80% of peak load. Yield point was measured from the load–displacement curve of the column. Two lines were made to intersect. A secant line passing through pre-peak segment of the curve at 65% of peak load was made to intersect the horizontal line tangent to the peak load. A vertical line was then drawn from the point of intersection, and its point of contact with the load–displacement curve was determined as the yield point. The yield strength ( $P_y$ ) and corresponding yield displacement ( $\Delta_{u,y}$ ) of all columns are produced in Table 11.

To facilitate the comparison between different column specimens, dimensionless normalized ratios of the mechanical properties of all columns with respect to that of control columns were calculated.

### 5.1. Residual Compressive Strength

The value of maximum residual compressive strength of all columns were normalized with respect to that of the control column. The ratio of peak compressive load of the column sample ( $P_{\max}$ ) to the peak compressive load of control column

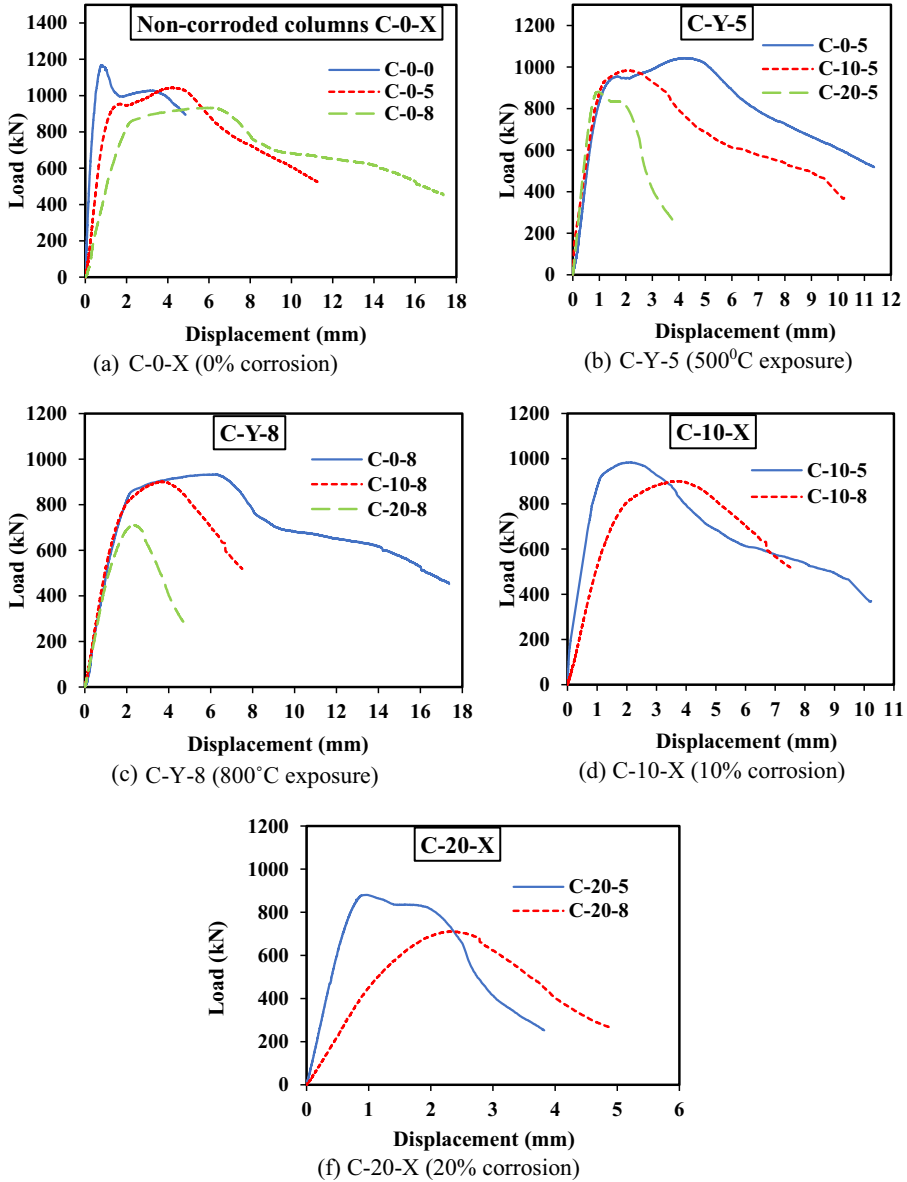


**Figure 12. Load-displacement curves of all columns.**

( $P_0$ ) was calculated for all column specimens. The results show that the peak load ratio  $P_{\max}/P_0$  varied from a maximum value of 1 to a minimum value of 0.61, i. e., a 39% reduction in peak compressive strength of column. The various values of the peak load ratios of columns were plotted and compared with each other as in Figs. 13, 14.

**Table 11**  
**Column Mechanical Test Results Summary**

Columns	Peak Load $P_{max}$ (kN)	Peak Load Ratio $(P_{max}/P_0)$	$\Delta u_{P_{max}}$ (mm)	$\varepsilon_{P_{max}}$ $/\varepsilon_{P_0}$	Yield Strength $P_y$ (kN)	$\Delta u_y$ (mm)	$0.8P_{max}$ (kN)	$\Delta u_{0.8P}$ (mm)	DF ( $\Delta$ )	DF Ratio
C-0-0	1168	1	0.8	1	1003.5	0.5	934.4	4.52	9.06	1
C-0-5	1043.6	0.89	4.22	5.32	892.82	1.17	834.99	6.48	5.54	0.61
C-0-8	933.29	0.79	6.28	7.94	826.28	2.03	747.49	8.31	4.1	0.45
C-10-5	983.63	0.84	2.12	2.68	843.67	0.94	787.24	4.04	4.34	0.47
C-20-5	880.6	0.75	0.96	1.21	798.7	0.71	704.4	2.39	3.37	0.37
C-10-8	901.3	0.77	3.7	4.67	765.4	1.76	721.6	5.84	3.32	0.36
C-20-8	710.9	0.61	2.31	2.91	621.9	1.61	568.4	3.3	2.06	0.22

For uncorroded samples, with increase in temperature of exposure, the value of peak load ratio was 0.89 for C-0-5 and 0.79 for C-0-8. For corroded columns with the same 10% degree of corrosion, with variation of temperature, the peak load ratio changed from 0.84 for column C-10-5 to 0.77 for C-10-8. For columns with 20% corrosion, with variation of temperature, the peak load ratio changed from 0.75 for C-20-5 to 0.6 for C-20-8. It signifies that the temperature of exposure affects the peak residual load value in all columns. Higher the temperature of exposure, more pronounced is the reduction in residual strength of the column.

For columns subjected to the same temperature of 500°C, with variation of degree of corrosion, the peak load ratio decreased from 0.89 for column C-0-5 to 0.84 for C-10-5, then to 0.75 for column C-20-5. Furthermore, for columns exposed to 800°C temperature, with increase in degree of corrosion, the peak load ratio reduced from 0.79 for C-0-8 to 0.77 for C-10-8, then to 0.6 for C-20-8. The results indicate that with temperature of exposure remaining same, while moderate level of corrosion results in reduction of peak residual strength of the column, as the level of corrosion increases, the peak residual strength is affected more profoundly compared to the effects of moderate level corrosion. Which is evident from the fact that while the reduction in the value of the peak load ratio was only 0.05 from C-0-5 to C-10-5 and only 0.02 from C-0-8 to C-10-8; it was as high as 0.14 from C-0-5 to C-20-5 and 0.19 from C-0-8 to C-20-8. Higher the temperature of exposure, less significant is the effect of moderate corrosion and more detrimental is the effect of higher corrosion degree on the value of residual compressive strength of the column.

## 5.2. Strain Ratio

The deflection corresponding to peak load  $\Delta u_{P_{max}}$  and the post peak deflection at which load drops to 80% of the peak load  $\Delta u_{0.8P}$  were noted down for all columns as shown in the Table 11. In order to characterize residual deformability of all columns, the values of deflection at peak load  $\Delta u_{P_{max}}$  and post peak deflection at 80% of the peak load  $\Delta u_{0.8P}$  of all samples were normalized with respect to the

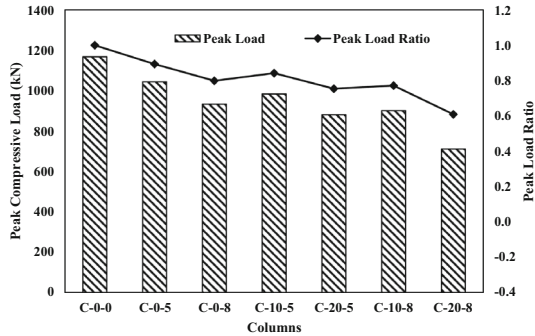


**Figure 13. Comparison of residual compressive strength of all columns.**

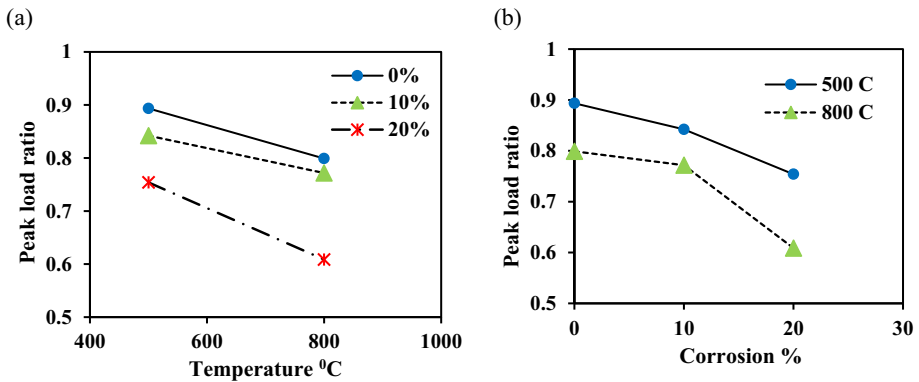


**Figure 14. Peak Load variation with (a) temperature; (b) degree of corrosion.**

corresponding deflection values of control column and were termed as strain ratios. Strain ratio at peak load of any column  $\varepsilon_{P_{max}} / \varepsilon_{P_0}$  was calculated as ratio of deflection at peak load of the column ( $\Delta u_{P_{max}}$ ) to the deflection at the peak load of control column ( $\Delta u_0$ ). Similarly post peak strain ratio of a column  $\varepsilon_{0.8P} / \varepsilon_{0.8P_0}$  was calculated as the ratio of deflection of the column when the load value drops to 80% of the peak load ( $\Delta u_{0.8P}$ ) to the deflection of the control column at 80% of peak load ( $\Delta u_{0.8P_0}$ ). The values of strain ratios of columns were plotted as shown in Figs. 15, 16, 17 for better clarification regarding the effect of different parameters on the strain ratio response of columns.

As can be seen from Fig. 16b, the temperature of exposure remaining same, the strain ratios of columns decreased with increasing degree of corrosion. While Fig. 16a illustrates that with degree of corrosion remaining same, the strain ratios increased with increasing temperature of exposure. Thus, the two parameters had opposing effects on the response of strain of the columns during axial compressive test.

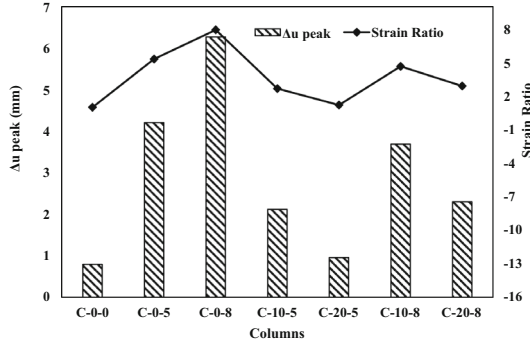


**Figure 15. Comparison of deflection and strain ratio at peak load of all columns.**

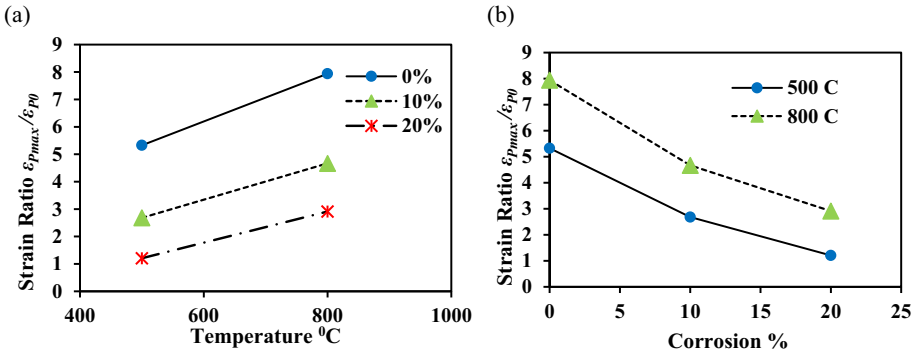


**Figure 16. Variation of strain ratio at peak load with (a) temperature; (b) degree of corrosion.**

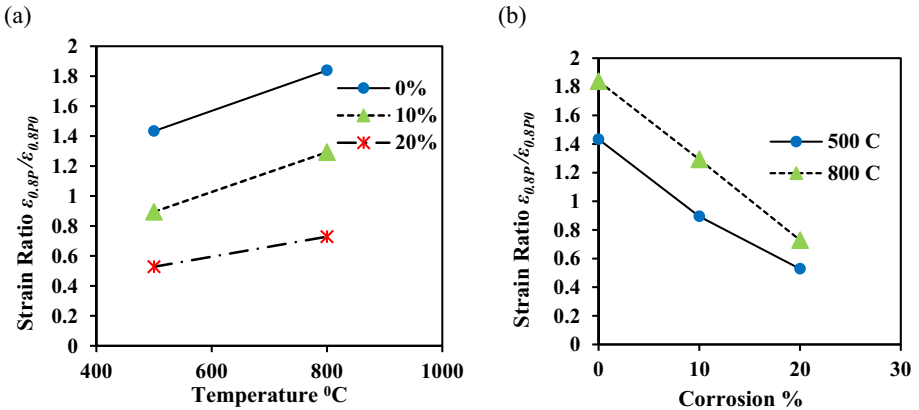


**Figure 17. Variation of strain ratio at 0.8\*peak load with (a) temperature; (b) degree of corrosion.**



The value of strain ratio at peak load  $\epsilon_{P_{max}} / \epsilon_{P0}$  for uncorroded columns increased from 1 for control column C-0-0 to 5.32 for C-0-5 and then to 7.94 for C-0-8. As the temperature of exposure increased, the strain ratio kept increasing for uncorroded columns. The physical and chemical changes in concrete due to exposure to higher temperature result in softening of concrete. The plots agreed with the observations in the literature, that during axial compression test, RC columns exposed to higher temperatures exhibited higher axial strain at peak load and flatter post peak section of load vs axial deflection curves [51]. Similar behaviour was observed for all heated columns in the current investigation. With the degree of corrosion remaining same, rise in temperature resulted in an increase in the value of  $\epsilon_{P_{max}} / \epsilon_{P0}$ . For 10% corroded columns, as the target temperature of exposure increased,  $\epsilon_{P_{max}} / \epsilon_{P0}$  increased from 2.68 for C-10-5 to 4.67 for C-10-8. Similarly for 20% corroded columns,  $\epsilon_{P_{max}} / \epsilon_{P0}$  increased from 1.21 for C-20-5 to 2.91 for C-20-8. It indicated that with increment in temperature of exposure remaining same, more severe the level of corrosion, lesser is the rise in value of strain ratio at peak load.

Similar trend followed for  $\epsilon_{0.8P} / \epsilon_{0.8P0}$  as is evident in Fig. 17. While for uncorroded columns, with rise in temperature of exposure, value of  $\epsilon_{0.8P} / \epsilon_{0.8P0}$  increased from 1 for Control column to 1.43 for C-0-5 and 1.84 for C-0-8. Corroded columns also showed similar pattern. For 10% corroded columns, value of  $\epsilon_{0.8P} / \epsilon_{0.8P0}$  increased from 0.89 for C-10-5 to 1.29 for C-10-8. Also, for 20% corroded columns there was a rise in value of  $\epsilon_{0.8P} / \epsilon_{0.8P0}$  from 0.53 for C-20-5 to 0.73 for C-20-8. It can be inferred that irrespective of degree of corrosion present in the columns, rise in temperature of exposure always results in increase in strain ratio at peak load as well as at post peak load when column strength drops to 80% of peak strength.

The effect of degree of corrosion on the strain ratio response of column was observed to be the reverse of the effect of thermal exposure on the same. With target temperature of exposure remaining same, with rise in degree of corrosion, the value of strain ratio  $\epsilon_{P_{max}} / \epsilon_{P0}$  reduced from 5.32 for C-0-5 to 2.68 for C-10-5, then to 1.21 for C-20-5. Furthermore, with target temperature remaining 800°C, with increase in degree of corrosion, the value of strain ratio  $\epsilon_{P_{max}} / \epsilon_{P0}$  reduced from 7.94 for C-0-8 to 4.67 for C-10-8 and a further reduction to 2.91 for C-20-8. The trend agreed with the observations of previous studies on corroded RC columns under axial compression test: reinforcement corrosion results in reduced peak compressive load and corresponding strain values; and steeper post peak curve indicating brittle behaviour of corroded columns [19]. Similar pattern was found for strain ratio  $\epsilon_{0.8P} / \epsilon_{0.8P0}$ . While target thermal exposure remained the same, with rise in degree of corrosion, the value of  $\epsilon_{0.8P} / \epsilon_{0.8P0}$  decreased from 0.89 for C-10-5 to 0.53 for C-20-5. It reduced from 1.29 for C-10-8 to 0.73 for C-20-8. Due to the presence of corrosion in RC columns, the lateral restraint provided by corroded stirrups reduced significantly, mechanical properties of longitudinal reinforcements degraded as well. These resulted in brittle failure of the columns. This might explain the decrease in the value of the strain corresponding to peak load in corroded columns. The normalized values of the peak load ratios, strain ratios and ductility factor ratios of all columns are mentioned in Table 11.

### 5.3. Ductility Factor

It was observed that the value of ductility factor ( $\Delta$ ) for columns gradually reduced with increasing damage to the column. An increase in temperature of exposure and a rise in degree of corrosion, both resulted in reduction of ductility factor (DF) for columns. The ductility factor for control column C-0-0 was as high as 9.06, which reduced to only 2.06 for the most damaged column C-20-8. For normalization, the ductility factor ratio for a column was measured as the ratio of the ductility factor of the column to that of the control column. The obtained values were plotted as shown in Figs.18, 19.

For uncorroded columns, with rise in temperature, the value of ductility factor ratio reduced from 1 for control column C-0-0 to 0.61 for C-0-5 to 0.45 for C-0-8. For corroded columns, the same trend was observed with rise in temperature, with a reduction of ductility factor ratio from 0.47 for C-10-5 to 0.37 for C-10-8 and from 0.36 for C-10-8 to 0.22 for C-20-8. A rise in degree of corrosion, with temperature of exposure remaining same, also resulted in further decline in the value of ductility factor ratio. It decreased from 0.47 for C-10-5 to 0.37 for C-20-5, and from 0.36 for C-10-8 to 0.22 for C-20-8. It is evident from the plots that temperature of exposure and degree of corrosion, both parameters had similar impact on the value of ductility factor ratio of the columns. The change in ductility factor ratio with increase in degree of corrosion, seems not to depend upon the temperature of exposure.

## 6. Conclusions

Main objective of this study was to evaluate the effect of corrosion on the behaviour of RC columns subjected to high temperature exposure. Based on the experimental results obtained, following conclusions can be summarized:

1. The maximum thermal gradient in columns increased with increase in target temperature of exposure, irrespective of the degree of corrosion. Further, the value of maximum thermal gradient was lower for corroded columns compared to non-corroded columns, subject to same thermal exposure. In addition, the time difference between attainment of maximum temperature at the centre of the column and the initiation of furnace cooling was observed to decrease with increase in degree of corrosion.
2. Transverse reinforcements are more damaged by accelerated corrosion process compared to longitudinal reinforcements as they are nearer to the surface of the column. Even at 10% targeted corrosion degree, there was significant loss of cross section in the stirrups. Thus, the functionality of stirrups for providing adequate lateral restraint and shear strength to the column is compromised. Columns with target corrosion level of 20% had few transverse reinforcements completely consumed at the corners, leaving the stirrups open-ended. It nullified the very purpose of the providing stirrups in the column. In such cases, the advantage of providing 135° bend in stirrup with its parts re-entering into core

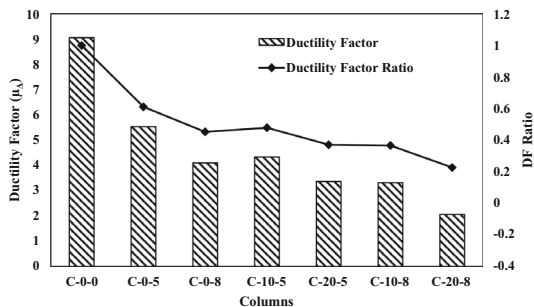


**Figure 18. Comparison of ductility factors for all columns.**

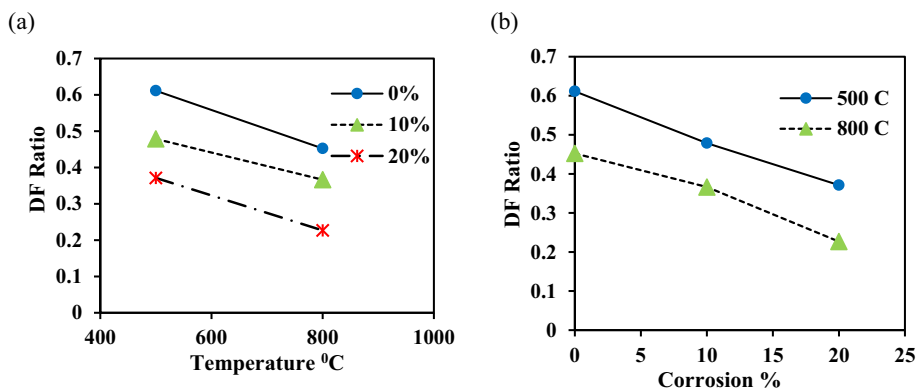


**Figure 19. Variation of ductility factor ratio with (a) temperature; (b) degree of corrosion.**

of concrete for better fire performance of RC columns, will also be rendered ineffective.

- Based on the observations from current study, proper cover should be ensured from the outer surface of the stirrups of the edged columns. Protection of stirrups from corrosion is vital for the proper functioning of columns. At the same time, enough precaution should be taken to protect stirrups from heat exposure as well. The cover thickness should be clearly specified from the surface of the stirrup, rather than from the longitudinal reinforcement. Role of stirrup design and layout seems crucial in this aspect, it should be further investigated extensively in future research studies.
- Pre-existing cracks in columns due to corrosion damage and thermal exposure determine the crack patterns during axial compression testing.
- The ultimate bearing capacity, the yield strength and the ductility factor of the columns reduced as the level of damage to the columns increased. Temperature of exposure and degree of corrosion both seemed to have similar impact on them. Whereas compared to the degree of corrosion, the exposure temperature had a more detrimental impact on the initial stiffness of the columns.

6. Rise in temperature resulted in an increase in the strain at peak load and post peak load irrespective of the degree of corrosion. While for the same target temperature of exposure, strain at peak load reduced with rise in degree of corrosion. Post peak section of load–displacement curves was getting flatter with rise in temperature of exposure and was getting steeper with rise in degree of corrosion indicating brittle failure. The physical and chemical changes in concrete due to exposure to high temperatures resulted in softening of concrete. While in the presence of corrosion in the columns, the mechanical properties of longitudinal bars and the lateral restraints provided by the stirrups reduced considerably. This might explain the opposing effects of corrosion and heat exposure on the strain at peak load of columns.
7. The pre-existing corrosion in the columns was the deciding factor while designing the heat exposure program. As the topic is at a nascent stage, considering the limited number of specimens, the highest level of heat exposure was designed so as not to cause a damage so severe to the columns, that it would have been difficult to record the proper load–deflection behaviour during axial compressive strength test. Even though the deviation of chosen thermal exposure from standard fire exposure was significant, the findings from current study are applicable to real life scenarios. Corroded RC columns will have compromised lateral restraint due to corrosion in stirrups, that will severely affect their load carrying capacities. As the study pointed out the difference of various mechanical properties and thermal gradients between pristine and corroded columns, the usual laboratory practice of testing pristine columns for predicting real fire scenarios in corroded RC columns will not furnish proper results.
8. Further research is recommended to investigate the impact of corrosion on the heat flow mechanisms in RC columns under elevated temperatures. Given the exploratory nature and available resources, the fire exposure in current study was taken artificially. Extensive studies incorporating wider range of parameters such as target temperatures, heating rates, standard fire exposure, more levels of degrees of corrosion, varying reinforcement detailing, testing in full-scale RC columns, etc. are recommended in this aspect to better understand the role of corrosion on the behaviour of RC columns exposed to high temperatures.

## Declarations

**Competing interest** The authors declare that they have no conflict of interests pertinent to the publication of furnished results in current study.

## References

1. Kumar D, Agrawal S, Sahoo D (2023) Assessment of the intrinsic bioremediation capacity of a complexly contaminated Yamuna River of India: a algae-specific approach. *Int J Phytorem* 25(13):1844–1858. [10.1080/15226514.2023.2200862](https://doi.org/10.1080/15226514.2023.2200862)
2. Ground Water Yearbook (2022) National Capital Territory, Delhi. 2021–2022. Government of India. Central Ground Water Board. State Unit Office, Delhi. Department of Water Resources, River Development & Ganga Rejuvenation. Ministry of Jal Shakti

3. Kuttippurath J, Peter R, Singh A, Raj S (2022) The increasing atmospheric CO<sub>2</sub> over India: comparison to global trends. *IScience* 25(8):104863. [10.1016/j.isci.2022.104863](https://doi.org/10.1016/j.isci.2022.104863)
4. Cairns J, Plizzari GA, Du YG, Law DW, Chiara F (2005) Mechanical properties of corrosion-damaged reinforcement. *ACI Mater J* 102(4):256–264
5. Uomoto T, Misra S (1988) Behaviour of concrete beams and columns in marine environment when corrosion of reinforcing bars takes place, ACI SP-109. In: *Proceedings of 2nd international conference on concrete in marine environment, Canada*, pp 127–146
6. Apostolopoulos C, a., & Papadakis, V. G. (2008) Consequences of steel corrosion on the ductility properties of reinforcement bar. *Constr Build Mater* 22(12):2316–2324. [10.1016/j.conbuildmat.2007.10.006](https://doi.org/10.1016/j.conbuildmat.2007.10.006)
7. Bhargava K, Ghosh AK, Mori Y, Ramanujam S (2007) Corrosion-induced bond strength degradation in reinforced concrete—analytical and empirical models. *Nucl Eng Des* 237(11):1140–1157. [10.1016/j.nucengdes.2007.01.010](https://doi.org/10.1016/j.nucengdes.2007.01.010)
8. Castel A, Francois R, Arliguie G (2000) Mechanical behaviour of corroded reinforced concrete beams—part 1: experimental study of corroded beams. *Mater Struct* 33(9):539–544
9. Malumbela G, Moyo P, Alexander M (2009) Behaviour of RC beams corroded under sustained service loads. *Constr Build Mater* 23:3346–3351
10. Kashani MM, Maddocks J, Dizaj EA (2019) Residual capacity of corroded reinforced concrete bridge components: state-of-the-art review. *J Bridg Eng* 24(7):03119001. [10.1061/\(asce\)be.1943-5592.0001429](https://doi.org/10.1061/(asce)be.1943-5592.0001429)
11. Rodriguez J, Ortega LM, Casal J (1996) Load bearing capacity of concrete columns with corroded reinforcement. In: *Proceedings of 4th SCI international symposium on corrosion of reinforcement in concrete construction, royal society of chemistry, Cambridge, UK*, pp 220–230
12. Revathy J, Suguna K, Raghunath PN (2009) Effect of corrosion damage on the ductility performance of concrete columns. *Am J Eng Appl Sci* 2(2):324–327. [10.3844/ajeassp.2009.324.327](https://doi.org/10.3844/ajeassp.2009.324.327)
13. Lee C, Bonacci JF, Thomas MDA, Maalej M, Khajehpour S, Hearn N, Pantazopoulou S, Sheikh S (2000) Accelerated corrosion and repair of reinforced concrete columns using carbon fibre reinforced polymer sheets. *Can J Civ Eng* 27(5):941–948. [10.1139/100-030](https://doi.org/10.1139/100-030)
14. Bae SW, Belarbi A, Myers JJ (2005) Performance of corrosion-damaged RC columns repaired by CFRP sheets. *ACI Spec Publ* 230:1447–1464
15. Tapan M, Aboutaha RS (2011) Effect of steel corrosion and loss of concrete cover on strength of deteriorated RC columns. *Constr Build Mater* 25(5):2596–2603. [10.1016/j.conbuildmat.2010.12.003](https://doi.org/10.1016/j.conbuildmat.2010.12.003)
16. Wang XH, Liang FY (2008) Performance of RC columns with partial length corrosion. *Nucl Eng Des* 238(12):3194–3202. [10.1016/j.nucengdes.2008.08.007](https://doi.org/10.1016/j.nucengdes.2008.08.007)
17. Xia J, Jin W-L, Li L-Y (2016) Performance of corroded reinforced concrete columns under the action of eccentric loads. *J Mater Civ Eng* 28(1):04015087. [10.1061/\(asce\)mt.1943-5533.0001352](https://doi.org/10.1061/(asce)mt.1943-5533.0001352)
18. Vu NS, Yu B, Li B (2017) Stress-strain model for confined concrete with corroded transverse reinforcement. *Eng Struct* 151:472–487. [10.1016/j.engstruct.2017.08.049](https://doi.org/10.1016/j.engstruct.2017.08.049)
19. Wu X, Chen L, Li H, Xu J (2019) Experimental study of the mechanical properties of reinforced concrete compression members under the combined action of sustained load and corrosion. *Constr Build Mater* 202:11–22. [10.1016/j.conbuildmat.2018.12.156](https://doi.org/10.1016/j.conbuildmat.2018.12.156)

20. Li Q, Huang L, Ye H, Fu C, Jin X (2020) Mechanical degradation of reinforced concrete columns corroded under sustained loads. *Int J Civil Eng* 18(8):883–901. [10.1007/s40999-020-00511-w](https://doi.org/10.1007/s40999-020-00511-w)
21. Meda A, Mostosi S, Rinaldi Z, Riva P (2014) Experimental evaluation of the corrosion influence on the cyclic behaviour of RC columns. *Eng Struct* 76:112–123
22. Rajput AS, Sharma UK (2018) Corroded reinforced concrete columns under simulated seismic loading. *Eng Struct* 171:453–463. [10.1016/J.ENGSTRUCT.2018.05.097](https://doi.org/10.1016/J.ENGSTRUCT.2018.05.097)
23. Janotka I, Mojumdar SC (2005) Thermal analysis at the evaluation of concrete damage by high temperatures. *J Therm Anal Calorim* 81(1):197–203. [10.1007/s10973-005-0767-6](https://doi.org/10.1007/s10973-005-0767-6)
24. Felicetti R, Gambarova PG, Meda A (2009) Residual behavior of steel rebars and R/C sections after a fire. *Constr Build Mater* 23(12):3546–3555
25. Phan LT (2008) Pore pressure and explosive spalling in concrete. *Mater Struct* 41(10):1623–1632. [10.1617/s11527-008-9353-2](https://doi.org/10.1617/s11527-008-9353-2)
26. Kodur VKR (2014) Properties of concrete at elevated temperatures. *ISRN Civil Eng* 2014:1–15. [10.1155/2014/468510](https://doi.org/10.1155/2014/468510)
27. Kodur V, McGrath R (2003) Fire endurance of high strength concrete columns. *Fire Technol* 39(1):73–87. [10.1023/A:1021731327822](https://doi.org/10.1023/A:1021731327822)
28. Kodur VKR, Phan L (2007) Critical factors governing the fire performance of high strength concrete systems. *Fire Saf J* 42:482–488. [10.1016/j.firesaf.2006.10.006](https://doi.org/10.1016/j.firesaf.2006.10.006)
29. Dotrepe J-C, Franssen J-M, Bruls A, Baus R, Vandeveld P, Minne R, van Nieuwenburg D, Lambotte H (1997) Experimental research on the determination of the main parameters affecting the behaviour of reinforced concrete columns under fire conditions. *Mag Concr Res* 49(179):117–127
30. Buch SH, Sharma UK (2019) Fire resistance of eccentrically loaded reinforced concrete columns. *Fire Technol* . [10.1007/s10694-019-00823-x](https://doi.org/10.1007/s10694-019-00823-x)
31. Shah AH, Sharma UK (2017) Fire resistance and spalling performance of confined concrete columns. *Constr Build Mater* 156:161–174. [10.1016/j.conbuildmat.2017.08.167](https://doi.org/10.1016/j.conbuildmat.2017.08.167)
32. Anderberg Y, Thelandersson S (1976) Stress and deformation characteristics of concrete at high temperatures. 2. Experimental investigation and material behaviour model. (Bulletin of Division of Structural Mechanics and Concrete Construction, Bulletin 54; Vol. Bulletin 54). Lund Institute of Technology
33. Lange D, Jansson R (2014) A comparison of an explicit and an implicit transient strain formulation for concrete in fire. *Fire Saf Sci* 11:572–583. [10.3801/IAFSS.FSS.11-572](https://doi.org/10.3801/IAFSS.FSS.11-572)
34. Pul S, Atasoy A, Senturk M, Hajirasouliha I (2021) Structural performance of reinforced concrete columns subjected to high-temperature and axial loading under different heating-cooling scenarios. *J Build Eng* 42:102477. [10.1016/J.JOBE.2021.102477](https://doi.org/10.1016/J.JOBE.2021.102477)
35. Chinthapalli HK, Sharma S, Agarwal A (2022) Fire behavior and modeling of short RC columns in pure axial compression: role of volume, configuration, and spacing of lateral reinforcement. *J Struct Eng (US)* 148(1):1–17. [10.1061/\(ASCE\)ST.1943-541X.0003224](https://doi.org/10.1061/(ASCE)ST.1943-541X.0003224)
36. Ba G, Miao J, Zhang W, Liu J (2019) Influence of reinforcement corrosion on fire performance of reinforced concrete beams. *Constr Build Mater* 213:738–747. [10.1016/J.CONBUILDMAT.2019.04.065](https://doi.org/10.1016/J.CONBUILDMAT.2019.04.065)
37. Porcari G, Zalok E, Isgor O (2012) Fire performance of corrosion-damaged reinforced concrete beams. *J Struct Fire Eng* 3:311–326
38. Sobhan K, Reddy DV, Martinez F (2020) Fire resistance of corroded high-strength structural concrete. *J Struct Fire Eng* . [10.1108/JSFE-10-2019-0033](https://doi.org/10.1108/JSFE-10-2019-0033)
39. Tariq F, Bhargava P (2021) Flexural behaviour of corroded RC beams exposed to fire. *Structures* 33:1366–1375. [10.1016/j.istruc.2021.05.025](https://doi.org/10.1016/j.istruc.2021.05.025)

40. Chandra S, Sharma UK, Green M, Gales J, Bhargava P (2023) Fire performance of corroded reinforced concrete columns. *Fire Technol* . [10.1007/s10694-023-01472-x](https://doi.org/10.1007/s10694-023-01472-x)
41. International Measures of Prevention, Application, and Economics of Corrosion Technologies Study (2016) by National Association of Corrosion Engineers, NACE International, Houston, Texas, USA
42. Schmitt G, Schütze M, Hays GF, Burns W, Han E-H, Pourbaix A, Jacobson G (2009) Global needs for knowledge dissemination, research, and development in materials deterioration and corrosion control. The World Corrosion Organization
43. Revie RW (2011) Uhlig's corrosion handbook, 3rd edn. Wiley, Hoboken
44. BIS (Bureau of Indian Standards) (2000b) Plain and reinforced concrete: code of practice. IS 456. New Delhi, India: BIS
45. IS 10262:2009. Indian concrete mix design guidelines (2009)
46. IS 8112:2013. Ordinary Portland cement, 43 grade—specification (Second Revision)
47. IS 383:2016. Coarse and fine aggregate for concrete—specification (Third Revision)
48. IS 516 (Part 1/Section 1): 2021. Hardened concrete—methods of test
49. Broomfield JP (2006) Corrosion of steel in concrete: understanding, investigation and repair, 2nd edn. Taylor and Francis, New York. [10.1201/9781482265491](https://doi.org/10.1201/9781482265491)
50. EN 1992-1-2:2004 Eurocode 2: design of concrete structures—Part 1–2: general rules—structural fire design. CEN
51. Khoury GA (2000) Effect of fire on concrete and concrete structures. *Prog Struct Mat Eng* 2(4):429–447. [10.1061/41016\(314\)299](https://doi.org/10.1061/41016(314)299)
52. Dougill JW (1968) Some effects of thermal volume changes on the properties and behavior of concrete. *Struct Concr Cem Concr Assoc Lond* 1968:499–513
53. Hertz KD (2005) Concrete strength for fire safety design. *Mag Concr Res* 57(8):445–453
54. Phan LT, Carino NJ (2002) Effects of test conditions and mixture proportions on behavior of high-strength concrete exposed to high temperatures. *ACI Mater J* . [10.14359/11317](https://doi.org/10.14359/11317)
55. Hager I (2013) Behaviour of cement concrete at high temperature. *Bull Pol Acad Sci* 61 (1):145–154. [10.2478/bpasts-2013-0013](https://doi.org/10.2478/bpasts-2013-0013)
56. ASTM G1-03(2017)e1 (2017) Standard practice for preparing, cleaning, and evaluating corrosion test specimens, vol 03.02, pp 1–9. <https://doi.org/10.1520/G0001-03R17E01>

**Publisher's Note** Springer Nature remains neutral with regard to jurisdictional claims in published maps and institutional affiliations.

Springer Nature or its licensor (e.g. a society or other partner) holds exclusive rights to this article under a publishing agreement with the author(s) or other rightsholder(s); author self-archiving of the accepted manuscript version of this article is solely governed by the terms of such publishing agreement and applicable law.